Title

A Computational Pipeline to Predict Cardiotoxicity

Journal

Circulation Research, 126(8)

ISSN

0009-7330

Authors

Yang, Pei-Chi
DeMarco, Kevin R
Aghasafari, Parya
et al.

Publication Date

2020-04-10

DOI

10.1161/circresaha.119.316404

Peer reviewed

HHS Public Access

Author manuscript

Circ Res. Author manuscript; available in PMC 2021 April 10.

Published in final edited form as:

Circ Res. 2020 April 10; 126(8): 947–964. doi:10.1161/CIRCRESAHA.119.316404.

A Computational Pipeline to Predict Cardiotoxicity: From the Atom to the Rhythm

Pei-Chi Yang[1,*], **Kevin R. DeMarco**[1,*], **Parya Aghasafari**[1], **Mao-Tsuen Jeng**[1], **John R. D. Dawson**[1], **Slava Bekker**[2], **Sergei Y. Noskov**[3], **Vladimir Yarov-Yarovoy**[4], **Igor Vorobyov**[4], **Colleen E. Clancy**[4]

[1]Pharmacology, University of California Davis, UNITED STATES

[2]Science and Engineering, American River College, UNITED STATES

[3]Centre for Molecular Simulations, University of Calgary, CANADA

[4]Physiology and Membrane Biology, University of California Davis, UNITED STATES

Abstract

Rationale—Drug-induced proarrhythmia is so tightly associated with prolongation of the QT interval that QT prolongation is an accepted surrogate marker for arrhythmia. But QT interval is too sensitive a marker and not selective, resulting in many useful drugs eliminated in drug discovery.

Objective—To predict the impact of a drug from the drug chemistry on the cardiac rhythm.

Methods and Results—In a new linkage, we connected atomistic scale information to protein, cell and tissue scales by predicting drug binding affinities and rates from simulation of ion channel and drug structure interactions and then used these values to model drug effects on the hERG channel. Model components were integrated into predictive models at the cell and tissue scales to expose fundamental arrhythmia vulnerability mechanisms and complex interactions underlying emergent behaviors. Human clinical data were used for model framework validation and showed excellent agreement, demonstrating feasibility of a new approach for cardiotoxicity prediction.

Conclusions—We present a multiscale model framework to predict electro-toxicity in the heart from the atom to the rhythm. Novel mechanistic insights emerged at all scales of the system, from the specific nature of proarrhythmic drug interaction with the hERG channel, to the fundamental cellular and tissue level arrhythmia mechanisms. Applications of machine learning indicate necessary and sufficient parameters that predict arrhythmia vulnerability. We expect that the model framework may be expanded to make an impact in drug discovery, drug safety screening for a variety of compounds and targets, and in a variety of regulatory processes.

Graphical Abstract

Address correspondence to: Dr. Colleen E. Clancy, Dr. Igor Vorobyov, Tel: 530-754-0254, ceclancy@ucdavis.edu, ivorobyov@ucdavis.edu.

*contributed equally.

DISCLOSURES

Drs. Colleen E. Clancy; Pei-Chi Yang; Kevin DeMarco; Igor V. Vorobyov; are named as inventors on a pending patent application filed by the University of California on the use of *in silico* methods for cardiotoxicity prediction.

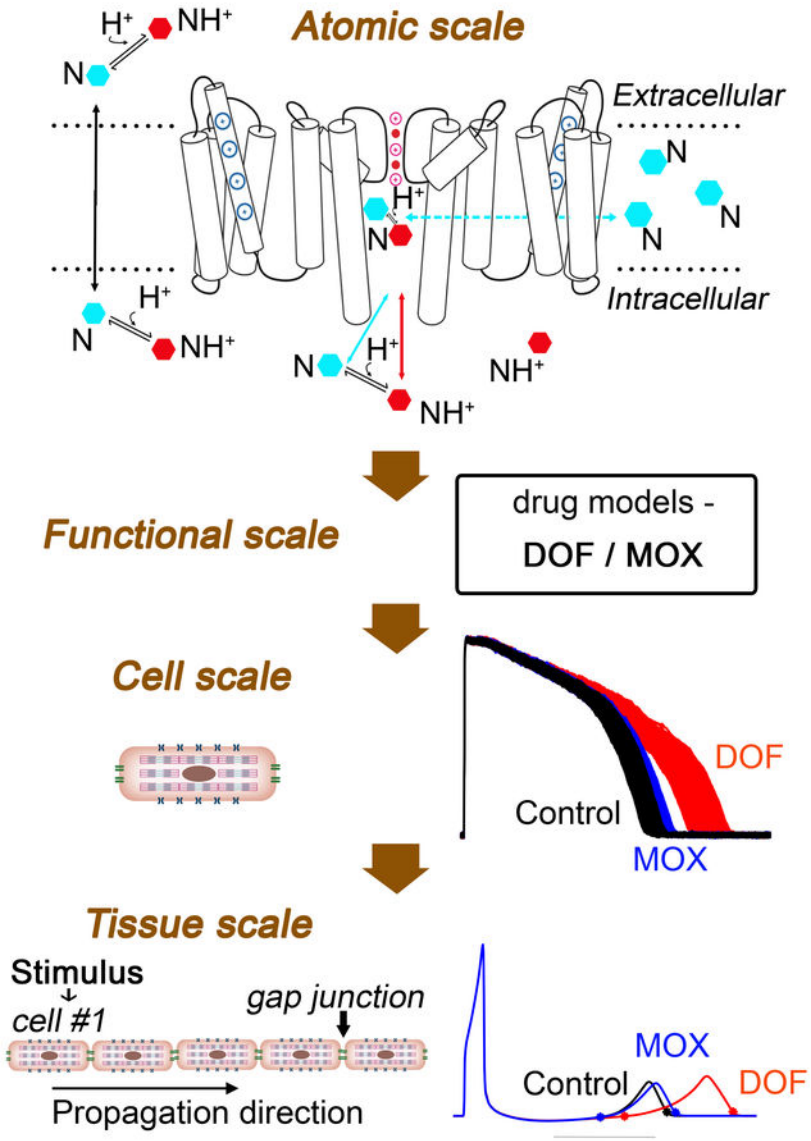

Keywords

Computational model; hERG; safety pharmacology; multiscale; drug-induced cardiotoxicity; cardiac arrhythmia; cardiac electrophysiology; computer-based model; HERG arrhythmia; Arrhythmias; Basic Science Research; Electrophysiology; Computational Biology; Pharmacology

INTRODUCTION

Cardiotoxicity is one of the most common reasons for drug removal from the market, typically manifesting as prolongation of the QT interval on the ECG and potential for fatal ventricular arrhythmias.[1] In the context of drug induced cardiac arrhythmia, the vital hindrance to prevention of electrical rhythm disturbances is a lack of meaningful approaches

to *distinguish between therapeutic, benign or harmful* actions of drugs. An important example is the use of QT interval prolongation as a surrogate marker for proarrhythmia.[2,3,4]

Abnormal cardiac electrical activity is most often a side effect from unintended block of the promiscuous drug target hERG, the delayed rectifier K^+ channel in the heart. hERG block results in prolongation of the QT interval on the ECG, a phase of the cardiac cycle that corresponds to ventricular repolarization. Numerous drugs interact with the promiscuous target hERG, and even seemingly innocuous agents such as grapefruit juice have been shown to prolong QT interval.[5] In the nearly 25 years since publication of the Survival With Oral d-sotalol (SWORD) trial showed that common antiarrhythmics increased mortality and risk of sudden cardiac death, no failsafe method has emerged to distinguish unsafe hERG blockers from safer drugs.[6–9]

There are at least two distinct classes of hERG blockers that prolong QT interval: Drugs that block hERG, prolong QT interval and increase proclivity to potentially deadly torsades de pointes (TdP) arrhythmias. This group includes, for instance, sotalol, dofetilide, [10, 11] and cisapride.[12] The second group consists of hERG blockers that prolong QT interval and have lower risk (in the absence of co-morbidities) for ventricular arrhythmias like moxifloxacin, ranolazine, and verapamil. [13–20] Importantly, FDA guidance does consider drug effects on the QT within a broader context of drug efficacy and utility for non-antiarrhythmic drugs.

The Comprehensive in Vitro Proarrhythmia Assay (CiPA) initiative comprising a team of regulators, academicians and industry scientists proposed a collection of nonclinical assays to move beyond the thorough-QT study and better predict preclinical arrhythmia risk.[21] This program promotes screening of additional cardiac ion channel targets and assessing net impact on the cellular action potential duration and QT interval via *in vitro* experiments and *in silico* functional models. While the consideration of multi-channel block is an improvement, even these newer computational models still generally rely on prolongation of the action potential duration or QT interval as the marker for safety.[22–26] Moreover, there is no mechanistic validation of the accuracy of the model prediction, so a test drug may land in the right category, but for the wrong reason. The *in silico* CiPA assay cannot distinguish between chemically similar drugs with similar affinity profiles. Moreover, incorporating individual genetic differences into the current model schema is not yet possible.

Although multichannel block is generally safer than hERG block alone, there are a variety of drugs that selectively target hERG and have been shown, in the absence of co-morbidities, [27, 28] to have lower arrhythmia risk than other hERG blockers. Lower risk hERG blockers include moxifloxacin and the selective-serotonin reuptake inhibitor CONA-437.[19, 20, 27, 29, 30] To be clear, while numerous studies have indicated a strong safety profile at clinically relevant serum concentrations in healthy individuals[18, 19], it has been demonstrated that in the presence of other QT prolonging risk factors, moxifloxacin has been indicated in torsades. [30–34] Moreover, some recent large scale population studies indicate increased risk, however, they uniformly acknowledge the failure to control for co-existent or concomitant risk factors. [2834] In this study, we focus on healthy human tissue, but future studies are planned to include disease states.

We hypothesized that channel conformational state specificity and the associated kinetics of hERG block may promote TdP as indicated by the TRIaD: *Triangulation*, *reverse* use dependence, beat-to-beat *instability* of action potential duration, temporal *and* spatial action potential duration *dispersion.*[10, 35, 36] Here, we use an integrative experimental and computational modeling and machine learning approach that spans scales from the atom to the cardiac rhythm. We predict intrinsic properties of the structure-activity relationship that determine proarrhythmia for the prototype drugs dofetilide and moxifloxacin, hERG blockers with different safety profiles: Dofetilide is a potent hERG blocker, prolongs QT interval and has a high risk for TdP arrhythmias.[37, 38] Moxifloxacin, on the other hand, is a safer drug in healthy individuals[19, 27, 30] (but has increased risk with concomitant comorbidities[27, 28]). Thus, these two drugs chosen as an ideal candidate for our proof-of-the-concept study.

In this study, we take the first necessary steps to answer the question, "*Can we predict hERG blocker proarrhythmic risk from the drug chemistry?"* We present a novel multiscale approach based on structural and dynamic atomistic models of drug-channel interactions and kinetics intended to predict drug-induced arrhythmia. The method can be also used to distinguish between chemically similar drugs that may appear to have similar effects on the action potential and QT interval, but differ in proarrhythmic risk.

METHODS

The data that support the findings of this study are available from the corresponding author upon reasonable request. Model codes have been made publicly available at Github. Please see the Major Resource Table in the Supplemental Materials.

A detailed description of Materials and Methods is available in the Online Supplemental Materials.

RESULTS

The first step towards predictive cardiac safety pharmacology was development of models of dofetilide and moxifloxacin. Both drugs have weakly basic or acidic functional groups and exist in different ionization states at physiological pH, with correspondingly different polarities, lipophilicities, and lipid membrane permeabilities. For this study, we developed and validated structural models for dofetilide (pK_a 7.0)[39] in neutral and cationic ionization states (Figure 1A), and moxifloxacin (pK_{a1} 6.25, pK_{a2} 9.29),[40] in neutral, cationic, and zwitterionic states (Figure 1E), compatible with biomolecular all-atom CHARMM force fields as described in Supplemental Materials.

We validated drug models by performing all-atom umbrella sampling molecular dynamics simulations across a hydrated 1-palmitoyl-2-oleoyl-sn-glycero-3-phosphocholine (POPC) lipid bilayer for dofetilide and a 1,2-dimyristoyl-sn-glycero-3-phosphocholine (DMPC) lipid bilayer for moxifloxacin, from which we computed one-dimensional free energy profiles, $\Delta G(z)$. There are substantial membrane perturbations as cationic dofetilide (Figure 1B) and zwitterionic moxifloxacin (Figure 1F) move towards the membrane center, and correspondingly energetic barriers for their membrane crossing are high (ΔG=15.8±0.1 and

ΔG=11.5±0.8 kcal/mol, see Figs. 1C and 1G, respectively). The energetic barriers were substantially lower for neutral dofetilide (ΔG=6.0±1.8 kcal/mol), cationic (ΔG=4.8±0.7 kcal/mol) and neutral (ΔG=3.2±0.3 kcal/mol) moxifloxacin, resulting in the shifts towards those drug ionization states in the membrane center, as shown in Figs. 1C and 1G. This along with their interfacial ΔG troughs suggests their membrane interface accumulation and higher rates of crossing compared to other ionization states.

To estimate membrane lipophilicities and crossing rates, we also computed one-dimensional diffusion coefficient profiles, $D(z)$, across membranes for each drug ionization state, indicating bulk water values (D_W) between ~6 $\times 10^{-6}$ and ~8 $\times 10^{-6}$ cm^2/s, that attenuate to D_M <0.5 $\times 10^{-6}$ cm^2/s at the membrane center (Figs. 1D and H), consistent with our previous studies.[41–43] We computed the water-membrane distribution coefficients for dofetilide ($\log D$ = 0.32±0.15) and moxifloxacin ($\log D$ = 0.13±0.11), and estimated the membrane translocation rate of neutral dofetilide as 8.0 ± 1.4 ms^{-1}, and neutral moxifloxacin as 1100 ± 580 ms^{-1}, and cationic moxifloxacin as 43 ± 29 ms^{-1} using Kramer's rate equation.[42] (see Supplemental Materials). For the cationic form of dofetilide and zwitterionic form of moxifloxacin, membrane crossing rates are expected to be several orders of magnitude smaller, and thus not contribute to membrane translocation within the simulated timescales.

In atomic scale simulations of drug interactions with the hERG open channel model (Figure 2A, 2C), we performed all-atom umbrella sampling simulations to compute one-dimensional free energy, ΔG, and diffusion coefficient, D, profiles (shown in Figure 2B and 2D). From these simulations we computed drug binding free energies (ΔG_{bind}) and dissociation constants (K_D) for multiple drug ionization states to the open hERG channel. The results reveal stronger binding of neutral dofetilide (Figure 2B), and neutral moxifloxacin (Figure 2D) in the channel pore compared to cationic or zwitterionic counterparts (see ΔG_{bind} in Figure 2E), and over an order of magnitude decrease in diffusion rates in the confined pore environment, for both drugs in each ionization state (Figure 2B and 2D, right). Accounting for relative fractions of cationic (38%) and neutral (62%) dofetilide forms at pH 7.2, using its pK_a value of 7.0[39], the overall K_D is estimated to be ~0.26 μM, which agrees favorably with IC_{50} values (3.5 μM, 10 μM, 11 μM) from electrophysiology experiments involving non-inactivating mutants of the channel or pulsing conditions disfavoring inactivated state[44–46]. Taking into account the dominant forms of moxifloxacin having relative fractions of cationic (10.33%), zwitterionic (83.99%) and neutral (5.68%) forms at pH 7.2.[40] the overall composite K_D is estimated to be ~13 μM, in agreement with available IC_{50} and K_D data (29 μM,[20] 64.5±10.3 μM,[47] 129 μM[48]) suggesting that moxifloxacin associates more selectively but less favorably to the open state than dofetilide[20]. We observed no free energy barriers for drug binding from bulk aqueous solution, suggesting that drug-channel "on" rates k_{on} will be diffusion limited. We also computed the z-dependent diffusion profiles into the hERG pore for multiple drug forms (Figure 2B and 2D, right). Diffusion coefficients in the intracellular bulk aqueous solution, D_W, were between ~6 $\times 10^{-6}$ cm^2/s and ~8 $\times 10^{-6}$ cm^2/s and attenuated to D_{pore} < 0.2 $\times 10^{-6}$ cm^2/s for both drugs near their binding sites. Comparing the diffusion coefficient profiles for drugs in the channel pore and membrane interior (see Figure 1D, 1H), diffusion there is an order of magnitude or more slower compared to bulk aqueous solution, due to a more viscous (membrane interior: 20-fold reduction) or constricted space (pore: 40-fold reduction). We computed k_{on} rates from free

energy (ΔG) and diffusion coefficient (D) profiles using the Debye-Smoluchowski equation[49, 50] (see Supplemental Materials), and they are similar for both drugs in each ionization state (see Figure 2E). Corresponding dissociation rates, k_{off}, computed as $k_{on} \cdot K_D$, are larger for cationic dofetilide and moxifloxacin, and zwitterionic moxifloxacin due to their weaker channel binding affinities (Figure 2E).

We next used the predicted values obtained from atomic scale simulations (Figure 3A) to seed a multiscale model of drug effects by first populating rate constants in a state dependent hERG function scale model shown schematically in Figure 3B and D for dofetilide and moxifloxacin, respectively. Dofetilide required optimization of one free parameter in the model due to a closed loop in the model (requirement for microscopic reversibility) arising from drug binding to the inactivated state.[18, 51–55]

Moxifloxacin on the other hand has not been shown to exhibit inactivated state block and so drug binding was not simulated to the inactivated state. Rather, moxifloxacin has been shown to inhibit hERG channels via a rate-independent open state blocking mechanism.[20, 48] It has also been shown that moxifloxacin does not rely strongly on binding to the S6 aromatic amino acid residues F656.[20] The absence of inactivated state block allowed for the model to be parameterized directly from the simulated data with no free parameters and consequently, no optimization was required.

For dofetilide, the “on” rates for open-inactivated state were free parameters and optimized to the experimentally obtained IC_{50} curve from Vicente et al.[56] by assuming that dofetilide binds 70-fold stronger to this channel state, i.e. $K_{DI} = (K_{Do} / 70)$[44] (Online Table III). In both experiment and simulations (Figure 3C), peak I_{Kr} was recorded at the end of the 3-s activating step to 0 mV with drug concentrations from 0 to 7.5 ng/mL. Percentage of drug block was calculated by $(I_{control} - I_{drug})*100/I_{control}$ and compared to experimental data,[56] demonstrating good fit (Figure 3C).

Figure 3D shows three modes of drug bound channel states – neutral (cyan), cationic (red), and zwitterionic (purple) for moxifloxacin. Our predicted (*no parameter optimization*) percentage of drug block was in remarkable agreement with experiments[20] as shown in Figure 3E.

Next, we subjected the model to a validation test using the gold standard data: human clinical data in the form of electrocardiograms in the absence and presence of dofetilide or moxifloxacin. To do so, as shown schematically in Figure 3A, we incorporated the function scale models of drug interaction with the hERG channel (Figure 3B and 3D) into the O’Hara-Rudy human cardiac ventricular myocyte model and then extended this model to construct a one-dimensional strand of O’Hara-Rudy cells.[57] We applied a simulated stimulus current at one end to initiate a propagating one-dimensional wave at the clinically reported heart rate between 43 and 75 beat per minute (bpm).[56] Figure 4A shows the computed heart rate corrected pseudo ECG (QT_C interval) for a range of dofetilide concentrations derived from signal averaged spatial and temporal gradients of electrical activity in the computational model. The red symbols are a comparison of human clinical data to model prediction following application of 2.72 ng/mL dofetilide.[10, 56]

Figure 4B shows the comparison of human clinical data from two studies (red and black lines) and model predictions (blue) under drug free conditions and following application of 2.72 ng/mL dofetilide.[10, 56] Each cell in the simulated tissue was subjected to a physiological noise current in order to introduce physiologically relevant inter-subject variability. The simulated mean values compared to clinically obtained data from humans are in excellent agreement, thereby providing an indication of the validity and predictive value of the computational pipeline to recapitulate the effect of a drug on the human QT interval.

In Figure 4C, we simulated QT intervals over a wide range of preceding RR intervals after 2.72 ng/mL dofetilide application and compared to the clinically observed changes[10] (with noise applied as above). Rate dependent changes in the QT interval were tracked as the slope of the linear regression line estimating the QT – $\sqrt{RR}$ relation. Again, the predicted relationship falls within the range of clinical data, indicating that the model can reproduce rate dependent changes in drug-induced QT interval. Finally, as shown in Figure 4D, our simulated effects of 2.5 mg/L moxifloxacin[58] on QT intervals are correctly predicted to fall within the range of multiple clinical data from humans.[59–65]

We next carried out computational screening in O'Hara-Rudy human computational ventricular myocytes for the effect of dofetilide or moxifloxacin to promote proarrhythmia by tracking key parameters as shown in Figure 5. We tracked each parameter in the absence of drug (control conditions in black) and in the presence of average patient plasma concentration of 2.72 ng/mL dofetilide (red), and 2.5 mg/L moxifloxacin (blue). To explore the effects of species differences we also simulated rabbit ventricular myocytes, which were similar to human (Online Figure I).

In Figure 5 the TRIaD was simulated. *Temporal APD dispersion* was quantified in a cell population of 1000 simulated cardiac myocyte action potentials by incorporating physiological noise.[66–68] Dofetilide within the clinical dosing range promotes temporal APD dispersion (maximum - minimum APD_{90}), while moxifloxacin has a subtle effect (Figure 5A: Control – 47 ms; 2.5 mg/L Moxifloxacin – 50 ms; 2.72 ng/mL Dofetilide – 78 ms). Figure 5B illustrates the effect of dofetilide and moxifloxacin to promote *triangulation* of the action potential as a function of APD prolongation. In the absence of drug, control cells had a slope of 0.25, while 2.5 mg/L moxifloxacin increased triangulation minimally to 0.34, while 2.72 ng/mL dofetilide increased the slope to 0.66. Figure 5C shows Poincaré plots of sequential APD pairs indicating beat-to-beat (bTb) *instability* following the application of small electrical perturbations in the absence of drug, with 2.5 mg/L moxifloxacin or with 2.72 ng/mL dofetilide. Instability was assessed by applying small amplitude inward currents randomly between -0.1 to −0.2 pA/pF for 50 ms over the course of the action potential plateau at a basic cycle length of 1000 ms. Dofetilide has a dramatic effect to increase instability, while moxifloxacin has a minor effect. In Figure 5D, *reverse use dependence* induced by dofetilide or moxifloxacin was evaluated. The curves were generated using APD_{90} values from human computational ventricular myocytes at steady-state at indicated frequencies. When dofetilide (red) was applied, there was a clear steepening of APD adaptation curve compared to drug-free (black) and moxifloxacin (blue). Panel E shows spatial dispersion of APD quantified in tissue by integrating the area under predicted T-wave

following a long pause (5000 ms). (See Supplemental Materials). Panel F shows profound increase in area (79%) under the T-wave when dofetilide is applied compared to moxifloxacin (9.4%).

We next used random forest machine learning to evaluate the importance of arrhythmia vulnerability parameters in the TRIaD to determine the final target classification (control versus drug-affected at different dofetilide and moxifloxacin doses). We used Pearson's correlation coefficient (see Supplemental Materials) to explore linear dependence of TRIaD parameters in Figure 5G, showing that TRIaD parameters are highly correlated. We then constructed a multiclass random forest classification (see Supplemental Materials) using correlated TRIaD parameters. The classifier indicates importance of each TRIaD parameter to correctly predict the target (drug free, medium or high risk) for two doses each of dofetilide and moxifloxacin. Figure 5H suggested that bTb *instability* is the most important feature to classify drug-affected cases into risk groups (see Supplemental Materials for details). Figure 5I illustrates the multiclassification for control, dofetilide 1.0 ng/mL, 2.72 ng/mL, moxifloxacin 2.5 mg/L, 4.73 mg/L using *bTb instability* and *T-wave area.* Random forest classification accuracy is 98%. This approach can be useful to compare the impact of changes in plasma concentrations and how they would be expected to affect relative risk, so called Anti-hERG activity.[69]

Arrhythmia is fundamentally an emergent spatial phenomenon. Accordingly, two-dimensional homogeneous (Figure 6, Panels A, B and C, endocardial cells) and heterogeneous (Figure 6, Panels D, E and F, endocardial region (cells 1 to 180) and epicardial region (cells 181 to 500)) anisotropic human ventricular *in silico* tissues (5 cm × 5 cm) with a linear decrease in APD as indicated by experimental data[70, 71] were simulated. Each simulated tissue contained randomized spatial heterogeneity imposed by the application of randomly applied low amplitude perturbations in the form of small inward currents, 0.1 to −0.45 pA/pF to *each cell* in the tissue at each time step for the duration of the simulation. In homogeneous tissue simulations in the absence and presence 2.5 mg/L moxifloxacin (Figure 6A and B), the tissue was very electrically stable, and normal cellular and tissue behavior is observed. However, 2.72 ng/ml dofetilide (Figure 6C) resulted in emergence of early afterdepolarizations (EADs) in some cells and not others, resulting in spatial dispersion of repolarization. As shown in D, E and F, the effect persisted when the tissue was heterogeneous (transmural heterogeneity), with considerably reduced dispersion of repolarization (as epicardial cells fire last, but repolarize first), and spatial repolarization gradients were observed only with dofetilide. These simulations suggest that in the presence of low levels of electrical instability, the application of a clinically relevant dose of dofetilide but not moxifloxacin promotes profound spatial dispersion of repolarization.

We next set out to test the effect of dofetilide and moxifloxacin in the setting of extrasystolic excitable triggers in heterogeneous tissue (Figure 7). With spatial noise to promote low-level electrical instability (described above), when 2D tissue was simulated using a typical S1-S2 protocol,[72, 73] 2.72 ng/ml dofetilide application resulted in dispersion of repolarization that was absent with moxifloxacin and drug free tissue. The tissue was paced (S1) (first panel) in a 0.5 cm × 1.1 cm area on the left edge of the endocardial region, and a premature stimulus S2 (third panel) was applied in a 1.8 cm × 1.5 cm area on the top left corner (endocardial

region). Time snapshots (panels) with voltage gradients indicated by the color map are shown in Figure 7. These maps were constructed following the last planar wave (S1) (first panel) and throughout termination of the most persistent wave after S2 stimulus (last panel). The corresponding action potentials from three points in space are shown in the right panels. Without drug (Figure 7A) or moxifloxacin application (Figure 7B) there was no persistence of electrical instability. In Figure 7C dofetilide reliably (n = 5 simulations) promoted persistent arrhythmia triggers observed as afterdepolarizations in cellular action potentials (right).

Finally, we developed an *in silico* left ventricular (LV) 3D wedge reconstruction of the human cardiac tissue based on the experimental data from Glukhov et al. [71] for the drug free case, with 2.72 ng/mL dofetilide and with 2.5 mg/L moxifloxacin applied. The LV wedges were paced at basic cycle of 750 ms for 20 beats with small amplitude inward currents randomly applied between -0.1 to −0.45 pA/pF to each cell after the ventricular activation. The model simulations show drug-induced QT interval prolongation both in male and female. However, in females, dofetilide caused considerably larger prolongation of the QT interval. This is consistent with clinical and experimental data suggest that male and female subjects respond differently to dofetilide intervention, with females exhibiting increased sensitivity and proclivity to abnormal rhythm [74–76]. A notable prediction from the model was that sex differences did not emerge following application of moxifloxacin under the conditions that we tested. This result is a prediction that can be tested in future experimental and clinical studies.

DISCUSSION

A major factor plaguing drug development is that there is no preclinical drug-screening tool that can accurately predict unintended drug induced cardiac arrhythmias from chemically similar drugs. The current approaches rely on substitute markers such as action potential duration or QT interval prolongation on the ECG. There is an urgent need to identify a new approach that can predict actual proarrhythmia from the drug chemistry rather than relying on surrogate indicators.

In this study we construct a computational pipeline for predictive safety pharmacology. The goal of this study was to develop a framework for detection of unsafe hERG blockers from their drug chemistry. Thus, we have assembled the process and utilized clinical data to demonstrate the utility for a proof-of-concept multiscale computational model to predict cardiac effects of dofetilide, a potent hERG blocker with a high pro-arrhythmia risk and moxifloxacin, which carries low arrhythmia risk in the absence of co-morbidities.[27, 28]

We began by developing physics-based computer models to account for channel conformational state and drug ionization state specific atomic-scale determinants of dofetilide and moxifloxacin interaction with hERG. This was accomplished through: 1) the development of open-state hERG atomistic structural model based on the published cryo-EM structure and validation via all-atom molecular dynamics simulations of K^+ conduction through the channel pore; 2) the development of empirical force field models for different ionization forms of dofetilide and moxifloxacin; 3) determination of free energy and

diffusion coefficient profiles for drug binding to the channel pore using enhanced sampling all-atom molecular dynamics simulations.

We utilized molecular dynamics simulations to predict association rates and affinities of dofetilide and moxifloxacin to the open state of the hERG K^+ channel. Interestingly, this approach yielded novel information about the nature of dofetilide interactions with hERG, suggesting that neutral dofetilide and moxifloxacin forms preferentially interact with the open channel state (see Figure 2B and 2D). Our previous function scale dofetilide model[77] was based on interpretation of experimental data. These data.[44,46,54] were used to estimate drug binding to the inactivated channel state in our model by assuming a 70-fold increase in predicted affinities from molecular dynamics simulations of the open state. Moxifloxacin required no such assumptions, and *remarkably, parameters derived from atomistic simulations yielded excellent prediction of dose response* (Figure 3E).

Our previous models required higher doses of dofetilide to cause prolongation of the QT interval,[77] but the model generated from the molecular dynamics generated parameters in this study was able to reproduce dose-dependent prolongation of the QT interval in very close agreement to the clinical data (Figure 4). In the physics-based approach that we used, the channel is restrained to stay in a particular conformation, allowing for an unambiguous calculation of drug-channel affinity for discrete channel conformational states. To ensure convergence of the calculated binding free energies we apply weak conformational restraints on the pore domain backbone atoms to keep the protein receptor structure in the open state. We based this assumption on the large body of prior theoretical work on the accurate computations of binding free energy from the all-atom free energy simulations [787980]. One of the major considerations in accurate evaluation of standard binding free energy for a flexible ligand to a receptor with multiple conformational state is to ensure efficient sampling of all states for the ligand itself to obtain work required for reversible binding/unbinding process from a very well-defined reference state of the receptor (with and without bound ligand). In addition to ensuring accurate calculations of the binding free energy for the ligand to a specific state, the presence of the conformational restraints on the receptor enables direct connections between calculated state-dependent binding affinity (K_D) and structural conformations of the channel implied by the Markov-model of hERG, e.g. open-activated and open-inactivated states. It is important to note that even within the restrained channel regime, atomistic simulation accounts for and includes protein flexibility within a given conformational state allowing adequate sampling of different drug - protein binding modes.

In this study we have attempted to make a novel link between ion channel structure and function. We utilized atomic scale predictions to inform rate constants for constructing computational channel-scale kinetic models for drug interaction with hERG channels. Calculations from drug – channel binding molecular-structure level trajectories allowed for the calculation of free energies and dissociation constants K_D for dofetilide and moxifloxacin interactions with the hERG open state. These simulated data combined with predicted diffusion coefficients from the same atomistic molecular dynamics runs allowed for drug “on” and “off” rates to discrete states to be introduced into the function scale Markov model of hERG. In this work we focused on physics-based models of drug binding

to an open conducting state based on available cryo-EM hERG structure [81] but drug interactions with inactivated and/or closed channel states and drug effect on conformational transitions between those states will be considered in subsequent studies.

Computational models of dofetilide and moxifloxacin interaction with the hERG receptor were integrated into virtual cardiac cell and tissue level models to predict emergent drug effects to promote elements of the TRIaD: Proarrhythmia markers that emerge at cell and tissue scales. The manifestation of the TRIaD parameters can be observed in the tissue level simulations designed to serve as *in silico* diagnostic indication of arrhythmia vulnerability. In Figs. 6 and 7, the model predictions show the emergence of arrhythmia triggers in the presence of low levels of applied electrical instability and dofetilide, but not moxifloxacin, in the absence and in the presence of extra stimuli as shown in Figure 7C.

Although it has long been clear that the TRIaD linked parameters indicate arrhythmia vulnerability,[10, 35, 36] it has not been clear which are the minimal and sufficient parameters to predict arrhythmia risk. Thus, we used random forest machine learning algorithm to evaluate the importance of each arrhythmia vulnerability parameter from the TRIaD to determine the final target classification. The Pearson's correlation coefficient indicated that all TRIaD parameters are highly correlated, thereby containing redundant information. Thus, we employed a multiclass random forest classification machine learning algorithm using the correlated TRIaD parameters to determine the relative importance of each to correctly predict whether a simulated cell belongs to the drug free, or low, medium or high risk category for a given drug and dose. The bTb *instability* parameter was shown to be most important feature in classifying the drug safety. Other drugs can be compared within this schema with outputs indicating relative risk, which may be useful in the context of FDA guidance as effective drug dose can be modified by physiological parameters that impact magnitude of channel block and pharmacokinetics. An example is the comparison of changes in free plasma concentrations and how they would be expected to affect relative risk, described as Anti-hERG activity.[69]

We investigated the impact of sex as a biological variable in drug induced arrhythmia vulnerability. In Figure 8, we show the impact of dofetilide and moxifloxacin on the male and female electrophysiology. Indeed, the model predictions are consistent with reported clinical data and show increased impact in the female case versus male following dofetilide application.[74, 75] Interestingly, we did not observe an impact of sex following moxifloxacin application under the conditions tested. This is a novel prediction of the model that can be expanded for a variety of testing conditions and that can be validated in future experimental or clinical studies. It should be noted that the male and female models here best represent the post-menopausal female and senescent male – we have not explicitly considered hormones during various phases of the menstrual cycle as we have done in previous studies.[82, 83] The male and female models were built from reported differences in male and female human explanted hearts that we utilized to inform the model development.[82, 84] However, even in senior men and women, substantial differences have been observed following dofetilide administration [74–76]. Future studies are planned to also predict the impact of sex steroid hormones in combination with drug application.

We brought together model simulations at the atomistic level for hERG channel structure, dynamics and channel – drug interactions as well as simulations at the functional levels of the protein, cell and tissue. *The power of combining these scales in a predictive framework is that it has allowed a way to derive on and off rates of drugs from atomic scale simulations and to then use these values to inform and build functional level channel models.* Function scale drug-channel models were then integrated into cellular and tissue level model to reveal mechanistic links between structure-activity relationships of ion channel – drug systems with higher order emergent electrical phenomena such as cardiac rhythm disturbances.

We anticipate the initial context of use for the technology presented here to be in the preclinical screening environment. Future efforts to automate and improve the efficiency of the process presented here will be required for use in industry, academic or regulatory setting. We must also undertake studies with compounds for which we are blinded to the proarrhythmia impact of the compounds until we have generated independent data that can be compared to *in vitro* and *in vivo* tests obtained by the safety pharmacology groups. The information required to do this is simply the chemical signature of the drug. From the drug chemistry, we can develop a model of the drug and the target and utilize simulation to predict rates that can populate parameters in the higher order models. This will constitute a key necessary validation step for the pipeline. Ultimately the added value of an *in silico* approach to drug screening is faster throughput and reduced cost. The approach can also be extended to other ion channel targets and G-protein coupled receptors as well as compounds that interact with multiple receptor targets and can be expanded to include varied genotypes and risk factors, and to predict individual responses to drug therapy.

There are limitations in the current state of the computational pipeline that should be noted. We did not take into account the pharmacokinetic and pharmacodynamic (PK/PD) profiles of drugs in this analysis, although PK/PD models could be linked to the models described here in a future study. Drug metabolism was not considered but is clearly a critical element that can be influenced by agents as varied as grapefruit to antifungal medication that may directly modify drug metabolic pathways or affect absorption rates. We did not account for multitarget effects of drugs and potential drug interactions, although the model might be expanded in future studies to include these elements. We made predictions in models that represent healthy human cardiac cells and tissue, but most reported incidences of drug-induced arrhythmia occur in the setting of concomitant co-morbidities.

Ultimately, the computational approach we present represents a scalable framework with automation potential to interact with other developing technologies,[85–90,91] and be applied to personalized medicine.[92] These technologies *in conjunction* with the multiscale models that we will develop may form *a process that can ultimately be used in the regulatory process prior to drug approval, in academia for research, in industry for drug and disease screening, and for clinical medicine.*

Supplementary Material

Refer to Web version on PubMed Central for supplementary material.

Acknowledgments

SOURCES OF FUNDING

NIH NHLBI 5R01HL128537-03 (CEC/VYY), NHLBI 5U01HL126273-04 (CEC/VYY/SYN). Canadian Institutes of Health Research Project Program Grant FRN-CIHR 156236 (SYN). ANTON PSCA17085P, PSCA16108P, PSCA18077P and PSCA17021P (IV/CEC/KRD/SYN), XSEDE MCB170095 (IV/KRD/CEC), SPARC 1OT2OD026580-01 (CEC/IV). AHA 16PRE27260295 (KRD), AHA 19CDA34770101 (IV), PMB Research Partnership Fund (IV/CEC), Team-based grant in Physiology (VYY/CEC), UC Davis Pharmacology T32GM099608 (JRDD). Compute Canada Resource Allocation Awards 2017–2019 (SYN), NCSA Blue Waters Broadening Participation Allocation (CEC/IV/KRD).

Nonstandard Abbreviations and Acronyms

AP	action potential
APD	action potential duration
bTb	beat-to-beat
CHARMM	Chemistry at Harvard Macromolecular Mechanics
CiPA	Comprehensive in Vitro Proarrhythmia Assay
DMPC	1,2-dimyristoyl-sn-glycero-3-phosphocholine
DOF	dofetilide
EAD	early afterdepolarizations
ECG	electrocardiogram
MOX	moxifloxacin
POPC	1-palmitoyl-2-oleoyl-sn-glycero-3-phosphocholine
TdP	torsades de pointes
TQT	Thorough QT Study
TRIaD	*Triangulation*, *reverse* use dependence, beat-to-beat *instability* of action potential duration, temporal *and* spatial action potential duration *dispersion*

REFERENCES

1. Roden DM. Drug-induced prolongation of the QT interval. The New England journal of medicine. 2004;350:1013–22. [PubMed: 14999113]
2. Hondeghem LM. QT prolongation is an unreliable predictor of ventricular arrhythmia. Heart Rhythm. 2008;5:1210–2. [PubMed: 18675236]
3. ICHHT. International Conference on Harmonisation Guidance on E14 clinical evaluation of QT/QTc interval prolongation and proarrhythmic potential for non-antiarrhythmic drugs;. Paper presented at: Notice Fed Regist; 2005.
4. ICH. Guidance for Industry: E14 Clinical Evaluation of QT/QTc Interval Prolongation and Proarrhythmic Potential for Non-Antiarrhythmic Drugs. 2005.

5. Chorin E, Hochstadt A, Granot Y, Khoury S, Schwartz AL, Margolis G, Barashi R, Viskin D, Ghantous E, Schnapper M, Mekori T, Fourey D, Guevara-Valdivia ME, Marquez MF, Zeltzer D, Rosso R and Viskin S. Grapefruit juice prolongs the QT interval of healthy volunteers and patients with long QT syndrome. Heart Rhythm. 2019;16:1141–1148. [PubMed: 31075442]
6. Cardiac Arrhythmia Suppression Trial III. Effect of the antiarrhythmic agent moricizine on survival after myocardial infarction. The New England journal of medicine. 1992;327:227–33. [PubMed: 1377359]
7. Waldo AL, Camm AJ, deRuyter H, Friedman PL, MacNeil DJ, Pauls JF, Pitt B, Pratt CM, Schwartz PJ and Veltri EP. Effect of d-sotalol on mortality in patients with left ventricular dysfunction after recent and remote myocardial infarction. The SWORD Investigators. Survival With Oral d-Sotalol. Lancet. 1996;348:7–12. [PubMed: 8691967]
8. Echt DS, Liebson PR, Mitchell LB, Peters RW, Obias-Manno D, Barker AH, Arensberg D, Baker A, Friedman L, Greene HL and et al. Mortality and morbidity in patients receiving encainide, flecainide, or placebo. The Cardiac Arrhythmia Suppression Trial. The New England journal of medicine. 1991;324:781–8. [PubMed: 1900101]
9. Lu HR, Rohrbacher J, Vlaminckx E, Van Ammel K, Yan GX and Gallacher DJ. Predicting drug-induced slowing of conduction and pro-arrhythmia: identifying the 'bad' sodium current blockers. Br J Pharmacol. 2010;160:60–76. [PubMed: 20331615]
10. Okada Y, Ogawa S, Sadanaga T and Mitamura H. Assessment of reverse use-dependent blocking actions of class III antiarrhythmic drugs by 24-hour Holter electrocardiography. J Am Coll Cardiol. 1996;27:84–9. [PubMed: 8522715]
11. Van Opstal JM, Leunissen JD, Wellens HJ and Vos MA. Azimilide and dofetilide produce similar electrophysiological and proarrhythmic effects in a canine model of Torsade de Pointes arrhythmias. Eur J Pharmacol. 2001;412:67–76. [PubMed: 11166738]
12. Wysowski DK and Bacsanyi J. Cisapride and fatal arrhythmia. The New England journal of medicine. 1996;335:290–1. [PubMed: 8657260]
13. Chorin E, Hu D, Antzelevitch C, Hochstadt A, Belardinelli L, Zeltser D, Barajas-Martinez H, Rozovski U, Rosso R, Adler A, Benhorin J and Viskin S. Ranolazine for Congenital Long-QT Syndrome Type III: Experimental and Long-Term Clinical Data. Circ Arrhythm Electrophysiol 2016;9.
14. Moreno JD, Yang PC, Bankston JR, Grandi E, Bers DM, Kass RS and Clancy CE. Ranolazine for congenital and acquired late INa-linked arrhythmias: in silico pharmacological screening. Circulation research. 2013;113:e50–e61. [PubMed: 23897695]
15. Li M and Ramos LG. Drug-Induced QT Prolongation And Torsades de Pointes. P T 2017;42:473–477. [PubMed: 28674475]
16. Melega MV, Alves M, Cavalcanti Lira RP, Cardoso da Silva I, Ferreira BG, Assis Filho HL, Pedreira Chaves FR, Martini AAF, Dias Freire LM, Reis RD and Leite Arieta CE. Safety and efficacy of intracameral moxifloxacin for prevention of post-cataract endophthalmitis: Randomized controlled clinical trial. J Cataract Refract Surg. 2019;45:343–350. [PubMed: 30691922]
17. Thomsen MB, Beekman JD, Attevelt NJ, Takahara A, Sugiyama A, Chiba K and Vos MA. No proarrhythmic properties of the antibiotics Moxifloxacin or Azithromycin in anaesthetized dogs with chronic-AV block. Br J Pharmacol. 2006;149:1039–48. [PubMed: 17088870]
18. Nalos L, Varkevisser R, Jonsson MK, Houtman MJ, Beekman JD, van der Nagel R, Thomsen MB, Duker G, Sartipy P, de Boer TP, Peschar M, Rook MB, van Veen TA, van der Heyden MA and Vos MA. Comparison of the IKr blockers moxifloxacin, dofetilide and E-4031 in five screening models of pro-arrhythmia reveals lack of specificity of isolated cardiomyocytes. Br J Pharmacol. 2012;165:467–78. [PubMed: 21718297]
19. Haverkamp W, Kruesmann F, Fritsch A, van Veenhuyzen D and Arvis P. Update on the cardiac safety of moxifloxacin. Curr Drug Saf 2012;7:149–63. [PubMed: 22873499]
20. Alexandrou AJ, Duncan RS, Sullivan A, Hancox JC, Leishman DJ, Witchel HJ and Leaney JL. Mechanism of hERG K+ channel blockade by the fluoroquinolone antibiotic moxifloxacin. Br J Pharmacol. 2006;147:905–16. [PubMed: 16474415]

21. Colatsky T, Fermini B, Gintant G, Pierson JB, Sager P, Sekino Y, Strauss DG and Stockbridge N. The Comprehensive in Vitro Proarrhythmia Assay (CiPA) initiative - Update on progress. J Pharmacol Toxicol Methods. 2016;81:15–20. [PubMed: 27282641]
22. Dutta S, Chang KC, Beattie KA, Sheng J, Tran PN, Wu WW, Wu M, Strauss DG, Colatsky T and Li Z. Optimization of an In silico Cardiac Cell Model for Proarrhythmia Risk Assessment. Front Physiol. 2017;8:616. [PubMed: 28878692]
23. Li Z, Dutta S, Sheng J, Tran PN, Wu W, Chang K, Mdluli T, Strauss DG and Colatsky T. Improving the In Silico Assessment of Proarrhythmia Risk by Combining hERG (Human Ether-a-go-go-Related Gene) Channel-Drug Binding Kinetics and Multichannel Pharmacology. Circ Arrhythm Electrophysiol. 2017;10:e004628. [PubMed: 28202629]
24. Grandi E, Morotti S, Pueyo E and Rodriguez B. Editorial: Safety Pharmacology - Risk Assessment QT Interval Prolongation and Beyond. Front Physiol. 2018;9:678. [PubMed: 29937733]
25. Passini E, Britton OJ, Lu HR, Rohrbacher J, Hermans AN, Gallacher DJ, Greig RJH, Bueno-Orovio A and Rodriguez B. Human In Silico Drug Trials Demonstrate Higher Accuracy than Animal Models in Predicting Clinical Pro-Arrhythmic Cardiotoxicity. Front Physiol. 2017;8:668. [PubMed: 28955244]
26. Li Z, Ridder BJ, Han X, Wu WW, Sheng J, Tran PN, Wu M, Randolph A, Johnstone RH, Mirams GR, Kuryshev Y, Kramer J, Wu C, Crumb WJ Jr, and Strauss DG. Assessment of an In Silico Mechanistic Model for Proarrhythmia Risk Prediction Under the CiPA Initiative. Clin Pharmacol Ther. 2019;105:466–475. [PubMed: 30151907]
27. Tulkens PM, Arvis P and Kruesmann F. Moxifloxacin safety: an analysis of 14 years of clinical data. Drugs R D. 2012;12:71–100. [PubMed: 22715866]
28. Cho Y and Park HS. Association of oral ciprofloxacin, levofloxacin, ofloxacin and moxifloxacin with the risk of serious ventricular arrhythmia: a nationwide cohort study in Korea. BMJ Open. 2018;8:e020974.
29. Alexandrou AJ, Milnes JT, Sun SZ, Fermini B, Kim SC, Jenkinson S, Leishman DJ, Witchel HJ, Hancox JC and Leaney JL. The human ether-a'-go-go related gene (hERG) K+ channel blockade by the investigative selective-serotonin reuptake inhibitor CONA-437: limited dependence on S6 aromatic residues. J Physiol Pharmacol. 2014;65:511–23. [PubMed: 25179083]
30. Khan F, Ismail M, Khan Q and Ali Z. Moxifloxacin-induced QT interval prolongation and torsades de pointes: a narrative review. Expert Opin Drug Saf. 2018;17:1029–1039. [PubMed: 30193085]
31. Sherazi S, DiSalle M, Daubert JP and Shah AH. Moxifloxacin-induced torsades de pointes. Cardiol J. 2008;15:71–3. [PubMed: 18651388]
32. Altin T, Ozcan O, Turhan S, Ongun Ozdemir A, Akyurek O, Karaoguz R and Guldal M. Torsade de pointes associated with moxifloxacin: a rare but potentially fatal adverse event. Can J Cardiol. 2007;23:907–8. [PubMed: 17876386]
33. Dale KM, Lertsburapa K, Kluger J and White CM. Moxifloxacin and torsade de pointes. Ann Pharmacother. 2007;41:336–40. [PubMed: 17284508]
34. Liu X, Ma J, Huang L, Zhu W, Yuan P, Wan R and Hong K. Fluoroquinolones increase the risk of serious arrhythmias: A systematic review and meta-analysis. Medicine (Baltimore). 2017;96:e8273. [PubMed: 29095256]
35. Hondeghem LM. TRIad: foundation for proarrhythmia (triangulation, reverse use dependence and instability). Novartis Found Symp. 2005;266:235–44; discussion 244–50. [PubMed: 16050272]
36. Hondeghem LM, Carlsson L and Duker G. Instability and triangulation of the action potential predict serious proarrhythmia, but action potential duration prolongation is antiarrhythmic. Circulation. 2001;103:2004–13. [PubMed: 11306531]
37. Abraham JM, Saliba WI, Vekstein C, Lawrence D, Bhargava M, Bassiouny M, Janiszewski D, Lindsay B, Militello M, Nissen SE, Poe S, Tanaka-Esposito C, Wolski K and Wilkoff BL. Safety of oral dofetilide for rhythm control of atrial fibrillation and atrial flutter. Circ Arrhythm Electrophysiol. 2015;8:772–6. [PubMed: 26063741]
38. Jaiswal A and Goldbarg S. Dofetilide induced torsade de pointes: mechanism, risk factors and management strategies. Indian Heart J. 2014;66:640–8. [PubMed: 25634399]
39. Cross PE, Arrowsmith JE, Thomas GN, Gwilt M, Burges RA and Higgins AJ. Selective class III antiarrhythmic agents. 1 Bis(arylalkyl)amines. J Med Chem. 1990;33:1151–5. [PubMed: 2319561]

40. Langlois MH, Montagut M, Dubost JP, Grellet J and Saux MC. Protonation equilibrium and lipophilicity of moxifloxacin. J Pharm Biomed Anal. 2005;37:389–93. [PubMed: 15708683]
41. Vorobyov I, Olson TE, Kim JH, Koeppe RE, 2nd, Andersen OS and Allen TW. Ion-induced defect permeation of lipid membranes. Biophys J. 2014;106:586–97. [PubMed: 24507599]
42. Boiteux C, Vorobyov I, French RJ, French C, Yarov-Yarovoy V and Allen TW. Local anesthetic and antiepileptic drug access and binding to a bacterial voltage-gated sodium channel. Proceedings of the National Academy of Sciences of the United States of America. 2014;111:13057–62. [PubMed: 25136136]
43. DeMarco KR, Bekker S, Clancy CE, Noskov SY and Vorobyov I. Digging into Lipid Membrane Permeation for Cardiac Ion Channel Blocker d-Sotalol with All-Atom Simulations. Front Pharmacol 2018;9:26. [PubMed: 29449809]
44. Perrin MJ, Kuchel PW, Campbell TJ and Vandenberg JI. Drug binding to the inactivated state is necessary but not sufficient for high-affinity binding to human ether-a-go-go-related gene channels. Mol Pharmacol. 2008;74:1443–52. [PubMed: 18701618]
45. Vijayvergiya V, Acharya S, Poulos J and Schmidt J. Single channel and ensemble hERG conductance measured in droplet bilayers. Biomed Microdevices. 2015;17:12. [PubMed: 25653065]
46. Weerapura M, Hebert TE and Nattel S. Dofetilide block involves interactions with open and inactivated states of HERG channels. Pflug Arch Eur J Phy. 2002;443:520–531.
47. Yu Z APIJ and Heitman LH. Kv 11.1 (hERG)-induced cardiotoxicity: a molecular insight from a binding kinetics study of prototypical Kv 11.1 (hERG) inhibitors. Br J Pharmacol. 2015;172:940–55. [PubMed: 25296617]
48. Kang J, Wang L, Chen XL, Triggle DJ and Rampe D. Interactions of a series of fluoroquinolone antibacterial drugs with the human cardiac K+ channel HERG. Mol Pharmacol. 2001;59:122–6. [PubMed: 11125032]
49. Debye P Reaction rates in ionic solutions. Transactions of the Electrochemical Society. 1942;82:265–272.
50. Shoup D and Szabo A. Role of diffusion in ligand binding to macromolecules and cell-bound receptors. Biophysical Journal. 1982;40:33–39. [PubMed: 7139033]
51. Weerapura M, Nattel S, Chartier D, Caballero R and Hebert TE. A comparison of currents carried by HERG, with and without coexpression of MiRP1, and the native rapid delayed rectifier current. Is MiRP1 the missing link? J Physiol. 2002;540:15–27. [PubMed: 11927665]
52. Ficker E, Jarolimek W, Kiehn J, Baumann A and Brown AM. Molecular determinants of dofetilide block of HERG K+ channels. Circulation research. 1998;82:386–95. [PubMed: 9486667]
53. Kiehn J, Lacerda AE, Wible B and Brown AM. Molecular physiology and pharmacology of HERG. Single-channel currents and block by dofetilide. Circulation. 1996;94:2572–9. [PubMed: 8921803]
54. Ishii K, Nagai M, Takahashi M and Endoh M. Dissociation of E-4031 from the HERG channel caused by mutations of an amino acid results in greater block at high stimulation frequency. Cardiovasc Res. 2003;57:651–9. [PubMed: 12618227]
55. Ishii K, Kondo K, Takahashi M, Kimura M and Endoh M. An amino acid residue whose change by mutation affects drug binding to the HERG channel. FEBS Lett. 2001;506:191–5. [PubMed: 11602243]
56. Vicente J, Johannesen L, Mason JW, Crumb WJ, Pueyo E, Stockbridge N and Strauss DG. Comprehensive T wave morphology assessment in a randomized clinical study of dofetilide, quinidine, ranolazine, and verapamil. J Am Heart Assoc. 2015;4.
57. O'Hara T, Virag L, Varro A and Rudy Y. Simulation of the undiseased human cardiac ventricular action potential: model formulation and experimental validation. PLoS computational biology. 2011;7:e1002061. [PubMed: 21637795]
58. Stass H, Dalhoff A, Kubitza D and Schuhly U. Pharmacokinetics, safety, and tolerability of ascending single doses of moxifloxacin, a new 8-methoxy quinolone, administered to healthy subjects. Antimicrob Agents Chemother. 1998;42:2060–5. [PubMed: 9687407]
59. Kligfield P, Green CL, Mortara J, Sager P, Stockbridge N, Li M, Zhang J, George S, Rodriguez I, Bloomfield D and Krucoff MW. The Cardiac Safety Research Consortium electrocardiogram

warehouse: thorough QT database specifications and principles of use for algorithm development and testing. Am Heart J. 2010;160:1023–8. [PubMed: 21146653]

60. Taubel J, Ferber G, Lorch U, Batchvarov V, Savelieva I and Camm AJ. Thorough QT study of the effect of oral moxifloxacin on QTc interval in the fed and fasted state in healthy Japanese and Caucasian subjects. Br J Clin Pharmacol. 2014;77:170–9. [PubMed: 23713767]
61. Morganroth J, Wang Y, Thorn M, Kumagai Y, Harris S, Stockbridge N, Kleiman R and Shah R. Moxifloxacin-induced QTc interval prolongations in healthy male Japanese and Caucasian volunteers: a direct comparison in a thorough QT study. Br J Clin Pharmacol. 2015;80:446–59. [PubMed: 26011050]
62. Panicker GK, Karnad DR, Kadam P, Badilini F, Damle A and Kothari S. Detecting moxifloxacin-induced QTc prolongation in thorough QT and early clinical phase studies using a highly automated ECG analysis approach. Br J Pharmacol. 2016;173:1373–80. [PubMed: 26784016]
63. Bloomfield DM, Kost JT, Ghosh K, Hreniuk D, Hickey LA, Guitierrez MJ, Gottesdiener K and Wagner JA. The effect of moxifloxacin on QTc and implications for the design of thorough QT studies. Clin Pharmacol Ther. 2008;84:475–80. [PubMed: 19238652]
64. Zhang X, Silkey M, Schumacher M, Wang L, Raval H and Caulfield JP. Period correction of the QTc of moxifloxacin with multiple predose baseline ECGs is the least variable of 4 methods tested. J Clin Pharmacol. 2009;49:534–9. [PubMed: 19287043]
65. Florian JA, Tornoe CW, Brundage R, Parekh A and Garnett CE. Population pharmacokinetic and concentration--QTc models for moxifloxacin: pooled analysis of 20 thorough QT studies. J Clin Pharmacol. 2011;51:1152–62. [PubMed: 21228407]
66. Sato D, Shiferaw Y, Garfinkel A, Weiss JN, Qu Z and Karma A. Spatially discordant alternans in cardiac tissue: role of calcium cycling. Circulation research. 2006;99:520–7. [PubMed: 16902177]
67. Tanskanen AJ and Alvarez LH. Voltage noise influences action potential duration in cardiac myocytes. Mathematical biosciences. 2007;208:125–46. [PubMed: 17174348]
68. Sato D, Bers DM and Shiferaw Y. Formation of Spatially Discordant Alternans Due to Fluctuations and Diffusion of Calcium. Plos One. 2013;8.
69. De Bruin ML, Pettersson M, Meyboom RH, Hoes AW and Leufkens HG. Anti-HERG activity and the risk of drug-induced arrhythmias and sudden death. European heart journal. 2005;26:590–7. [PubMed: 15637086]
70. Lou Q, Fedorov VV, Glukhov AV, Moazami N, Fast VG and Efimov IR. Transmural heterogeneity and remodeling of ventricular excitation-contraction coupling in human heart failure. Circulation. 2011;123:1881–90. [PubMed: 21502574]
71. Glukhov AV, Fedorov VV, Lou Q, Ravikumar VK, Kalish PW, Schuessler RB, Moazami N and Efimov IR. Transmural dispersion of repolarization in failing and nonfailing human ventricle. Circulation research. 2010;106:981–91. [PubMed: 20093630]
72. Liu J and Laurita KR. The mechanism of pause-induced torsade de pointes in long QT syndrome. Journal of cardiovascular electrophysiology. 2005;16:981–7. [PubMed: 16174020]
73. Yan GX, Wu Y, Liu T, Wang J, Marinchak RA and Kowey PR. Phase 2 early afterdepolarization as a trigger of polymorphic ventricular tachycardia in acquired long-QT syndrome : direct evidence from intracellular recordings in the intact left ventricular wall. Circulation. 2001;103:2851–6. [PubMed: 11401944]
74. Pokorney SD, Yen DC, Campbell KB, Allen LaPointe NM, Sheng S, Thomas L, Bahnson TD, Daubert JP, Picini JP, Jackson KP, Thomas KL and Al-Khatib SM. Dofetilide dose reductions and discontinuations in women compared with men. Heart Rhythm. 2018;15:478–484. [PubMed: 29605013]
75. Vorobyov I and Clancy CE. Sex, drugs, and funky rhythms. Heart Rhythm. 2018;15:485–486. [PubMed: 29605014]
76. Yang PC, Perissinotti LL, Lopez-Redondo F, Wang Y, DeMarco KR, Jeng MT, Vorobyov I, Harvey RD, Kurokawa J, Noskov SY and Clancy CE. A multiscale computational modelling approach predicts mechanisms of female sex risk in the setting of arousal-induced arrhythmias. J Physiol. 2017;595:4695–4723. [PubMed: 28516454]

77. Romero L, Trenor B, Yang PC, Saiz J and Clancy CE. In silico screening of the impact of hERG channel kinetic abnormalities on channel block and susceptibility to acquired long QT syndrome. J Mol Cell Cardiol. 2014;72:126–37. [PubMed: 24631769]

78. Lau AY and Roux B. The hidden energetics of ligand binding and activation in a glutamate receptor. Nat Struct Mol Biol. 2011;18:283–7. [PubMed: 21317895]

79. Hu X, Wang Y, Hunkele A, Provasi D, Pasternak GW and Filizola M. Kinetic and thermodynamic insights into sodium ion translocation through the mu-opioid receptor from molecular dynamics and machine learning analysis. PLoS computational biology. 2019;15:e1006689. [PubMed: 30677023]

80. Lenaeus MJ, Gamal El-Din TM, Ing C, Ramanadane K, Pomes R, Zheng N and Catterall WA. Structures of closed and open states of a voltage-gated sodium channel. Proceedings of the National Academy of Sciences of the United States of America. 2017;114:E3051–E3060. [PubMed: 28348242]

81. Wang W and MacKinnon R. Cryo-EM Structure of the Open Human Ether-a-go-go-Related K+ Channel hERG. Cell. 2017;169:422–430 e10. [PubMed: 28431243]

82. Yang PC and Clancy CE. In silico Prediction of Sex-Based Differences in Human Susceptibility to Cardiac Ventricular Tachyarrhythmias. Front Physiol 2012;3:360. [PubMed: 23049511]

83. Yang PC, Kurokawa J, Furukawa T and Clancy CE. Acute effects of sex steroid hormones on susceptibility to cardiac arrhythmias: a simulation study. PLoS computational biology. 2010;6:e1000658. [PubMed: 20126530]

84. Gaborit N, Varro A, Le Bouter S, Szuts V, Escande D, Nattel S and Demolombe S. Gender-related differences in ion-channel and transporter subunit expression in non-diseased human hearts. J Mol Cell Cardiol. 2010;49:639–46. [PubMed: 20600101]

85. Bridal TR, Margulis M, Wang X, Donio M and Sorota S. Comparison of human Ether-a-go-go related gene screening assays based on IonWorks Quattro and thallium flux. Assay and drug development technologies. 2010;8:755–65. [PubMed: 20658944]

86. Jow F, Shen R, Chanda P, Tseng E, Zhang H, Kennedy J, Dunlop J and Bowlby MR. Validation of a medium-throughput electrophysiological assay for KCNQ2/3 channel enhancers using IonWorks HT. Journal of biomolecular screening. 2007;12:1059–67. [PubMed: 18087070]

87. Harmer AR, Abi-Gerges N, Easter A, Woods A, Lawrence CL, Small BG, Valentin JP and Pollard CE. Optimisation and validation of a medium-throughput electrophysiology-based hNav1.5 assay using IonWorks. Journal of pharmacological and toxicological methods. 2008;57:30–41. [PubMed: 17980627]

88. Bridgland-Taylor MH, Hargreaves AC, Easter A, Orme A, Henthorn DC, Ding M, Davis AM, Small BG, Heapy CG, Abi-Gerges N, Persson F, Jacobson I, Sullivan M, Albertson N, Hammond TG, Sullivan E, Valentin JP and Pollard CE. Optimisation and validation of a medium-throughput electrophysiology-based hERG assay using IonWorks HT. Journal of pharmacological and toxicological methods. 2006;54:189–99. [PubMed: 16563806]

89. Sorota S, Zhang XS, Margulis M, Tucker K and Priestley T. Characterization of a hERG screen using the IonWorks HT: comparison to a hERG rubidium efflux screen. Assay and drug development technologies. 2005;3:47–57. [PubMed: 15798395]

90. Schroeder K, Neagle B, Trezise DJ and Worley J. Ionworks HT: a new high-throughput electrophysiology measurement platform. Journal of biomolecular screening. 2003;8:50–64. [PubMed: 12854998]

91. Nattel S and Carlsson L. Innovative approaches to anti-arrhythmic drug therapy. Nature reviews Drug discovery. 2006;5:1034–49. [PubMed: 17139288]

92. Braam SR, Tertoolen L, van de Stolpe A, Meyer T, Passier R and Mummery CL. Prediction of drug-induced cardiotoxicity using human embryonic stem cell-derived cardiomyocytes. Stem cell research. 2010;4:107–16. [PubMed: 20034863]

93. Faber GM and Rudy Y. Action potential and contractility changes in [Na(+)](i) overloaded cardiac myocytes: a simulation study. Biophys J. 2000;78:2392–404. [PubMed: 10777735]

94. Stramba-Badiale M, Locati EH, Martinelli A, Courville J and Schwartz PJ. Gender and the relationship between ventricular repolarization and cardiac cycle length during 24-h Holter recordings. European heart journal. 1997;18:1000–6. [PubMed: 9183593]

95. Nakagawa M, Ooie T, Ou B, Ichinose M, Takahashi N, Hara M, Yonemochi H and Saikawa T. Gender differences in autonomic modulation of ventricular repolarization in humans. Journal of cardiovascular electrophysiology. 2005;16:278–84. [PubMed: 15817086]

96. Ebert SN, Liu XK and Woosley RL. Female gender as a risk factor for drug-induced cardiac arrhythmias: evaluation of clinical and experimental evidence. Journal of women's health / the official publication of the Society for the Advancement of Women's Health Research. 1998;7:547–57.

97. Gima K and Rudy Y. Ionic current basis of electrocardiographic waveforms: a model study. Circulation research. 2002;90:889–96. [PubMed: 11988490]

98. Fridericia LS. The duration of systole in the electrocardiogram of normal subjects and of patients with heart disease. Acta Medica Scandinavica. 1920;53:469–86.

99. Young RJ and Panfilov AV. Anisotropy of wave propagation in the heart can be modeled by a Riemannian electrophysiological metric. Proceedings of the National Academy of Sciences of the United States of America. 2010;107:15063–8. [PubMed: 20696934]

100. Voit EO. Computational analysis of biochemical systems: a practical guide for biochemists and molecular biologists. Cambridge, New York: Cambridge University Press; 2000.

101. Syrjala MT, Liewendahl K, Valtonen V, Taavitsainen M and Gripenberg J. Sensitivity of 111In-granulocyte scintigraphy in various local infections. Acta Radiol. 1987;28:549–53. [PubMed: 2960346]

102. Saeys Y, Inza I and Larranaga P. A review of feature selection techniques in bioinformatics. Bioinformatics. 2007;23:2507–17. [PubMed: 17720704]

103. Rodgers JL and Nicewander WA. Thirteen Ways to Look at the Correlation Coefficient. The American Statistician. 1988;42:59–66.

104. Liaw A and Wiener MC. Classification and Resression by randomForest. R news. 2/3:18–22.

105. Breiman L Classification and regression trees: Routledge; 2017.

106. Grus J Data science from scratch: first principles with python: O'Reilly Media, Inc; 2015.

107. Andre I, Bradley P, Wang C and Baker D. Prediction of the structure of symmetrical protein assemblies. Proceedings of the National Academy of Sciences of the United States of America. 2007;104:17656–61. [PubMed: 17978193]

108. Yarov-Yarovoy V, Schonbrun J and Baker D. Multipass membrane protein structure prediction using Rosetta. Proteins. 2006;62:1010–25. [PubMed: 16372357]

109. Barth P, Schonbrun J and Baker D. Toward high-resolution prediction and design of transmembrane helical protein structures. Proceedings of the National Academy of Sciences of the United States of America. 2007;104:15682–7. [PubMed: 17905872]

110. Jo S, Kim T, Iyer VG and Im W. CHARMM-GUI: a web-based graphical user interface for CHARMM. J Comput Chem. 2008;29:1859–65. [PubMed: 18351591]

111. Brooks BR, Bruccoleri RE, Olafson BD, States DJ, Swaminathan Sa M. CHARMM: a program for macromolecular energy, minimization, and dynamics calculations. Journal of computational chemistry. 1983;4:187–217.

112. Brooks BR, Brooks III CL, Mackerell AD Jr, Nilsson L, Petrella RJ, Roux B, Won Y, Archontis G, Bartels C and Boresch S. CHARMM: the biomolecular simulation program. Journal of computational chemistry. 2009;30:1545–1614. [PubMed: 19444816]

113. Phillips JC, Braun R, Wang W, Gumbart J, Tajkhorshid E, Villa E, Chipot C, Skeel RD, Kale L and Schulten K. Scalable molecular dynamics with NAMD. Journal of Computational Chemistry. 2005;26:1781–1802. [PubMed: 16222654]

114. Shaw DE, Grossman JP, Bank JA, Batson B, Butts JA, Chao JC, Deneroff MM, Dror RO, Even A, Fenton CH, Forte A, Gagliardo J, Gill G, Greskamp B, Ho CR, Ierardi DJ, Iserovich L, Kuskin JS, Larson RH, Layman T, Lee LS, Lerer AK, Li C, Killebrew D, Mackenzie KM, Mok SYH, Moraes MA, Mueller R, Nociolo LJ, Peticolas JL, Quan T, Ramot D, Salmon JK, Scarpazza DP, Ben Schafer U, Siddique N, Snyder CW, Spengler J, Tang PTP, Theobald M, Toma H, Towles B, Vitale B, Wang SC and Young C. Anton 2: Raising the bar for performance and programmability in a special-purpose molecular dynamics supercomputer. Int Conf High Perfor 2014:41–53.

115. Huang J and MacKerell AD Jr., CHARMM36 all-atom additive protein force field: validation based on comparison to NMR data. J Comput Chem. 2013;34:2135–45. [PubMed: 23832629]

116. Klauda JB, Venable RM, Freites JA, O'Connor JW, Tobias DJ, Mondragon-Ramirez C, Vorobyov I, MacKerell AD, Jr. and Pastor RW. Update of the CHARMM all-atom additive force field for lipids: validation on six lipid types. J Phys Chem B. 2010;114:7830–43. [PubMed: 20496934]

117. Beglov D and Roux B. Finite Representation of an Infinite Bulk System - Solvent Boundary Potential for Computer-Simulations. J Chem Phys. 1994;100:9050–9063.

118. Jorgensen WL, Chandrasekhar J, Madura JD, Impey RW and Klein ML. Comparison of Simple Potential Functions for Simulating Liquid Water. J Chem Phys. 1983;79:926–935.

119. Vanommeslaeghe K, Hatcher E, Acharya C, Kundu S, Zhong S, Shim J, Darian E, Guvench O, Lopes P, Vorobyov I and MacKerell AD. CHARMM General Force Field: A Force Field for Drug-Like Molecules Compatible with the CHARMM All-Atom Additive Biological Force Fields. Journal of Computational Chemistry. 2010;31:671–690. [PubMed: 19575467]

120. Feller SE, Zhang Y, Pastor RW and Brooks BR. Constant pressure molecular dynamics simulation: The Langevin piston method. The Journal of Chemical Physics. 1995;103:4613–4621.

121. Nosé S A unified formulation of the constant temperature molecular dynamics methods. The Journal of Chemical Physics. 1984;81:511–519.

122. Hoover WG. Canonical dynamics: Equilibrium phase-space distributions. Physical Review A. 1985;31:1695–1697.

123. Ryckaert J-P, Ciccotti G and Berendsen HJC. Numerical integration of the cartesian equations of motion of a system with constraints: molecular dynamics of n-alkanes. Journal of Computational Physics. 1977;23:327–341.

124. Darden T, York D and Pedersen L. Particle mesh Ewald: An N·log(N) method for Ewald sums in large systems. The Journal of Chemical Physics. 1993;98:10089–10092.

125. Long SB, Tao X, Campbell EB and MacKinnon R. Atomic structure of a voltage-dependent K+ channel in a lipid membrane-like environment. Nature. 2007;450:376–82. [PubMed: 18004376]

126. Vanommeslaeghe K and MacKerell AD. Automation of the CHARMM General Force Field (CGenFF) I: Bond Perception and Atom Typing. J Chem Inf Model. 2012;52:3144–3154. [PubMed: 23146088]

127. Vanommeslaeghe K, Raman EP and MacKerell AD. Automation of the CHARMM General Force Field (CGenFF) II: Assignment of Bonded Parameters and Partial Atomic Charges. J Chem Inf Model. 2012;52:3155–3168. [PubMed: 23145473]

128. Mayne CG, Saam J, Schulten K, Tajkhorshid E and Gumbart JC. Rapid Parameterization of Small Molecules Using the Force Field Toolkit. Journal of Computational Chemistry. 2013;34:2757–2770. [PubMed: 24000174]

129. Humphrey W, Dalke A and Schulten K. VMD: visual molecular dynamics. J Mol Graph. 1996;14:33-8, 27-8. [PubMed: 8744570]

130. Frisch M, Trucks G, Schlegel H, Scuseria G, Robb M, Cheeseman J, Scalmani G, Barone V, Mennucci B and Petersson G. Gaussian 09. Wallingford, CT: Gaussian 2009.

131. Torrie GM and Valleau JP. Nonphysical sampling distributions in Monte Carlo free-energy estimation: Umbrella sampling. Journal of Computational Physics. 1977;23:187–199.

132. Kumar S, Rosenberg JM, Bouzida D, Swendsen RH and Kollman PA. THE weighted histogram analysis method for free-energy calculations on biomolecules. I. The method. Journal of Computational Chemistry. 1992;13:1011–1021.

133. Hummer G Position-dependent diffusion coefficients and free energies from Bayesian analysis of equilibrium and replica molecular dynamics simulations. New Journal of Physics. 2005;7:34.

134. Vorobyov I, Bennett WF, Tieleman DP, Allen TW and Noskov S. The Role of Atomic Polarization in the Thermodynamics of Chloroform Partitioning to Lipid Bilayers. J Chem Theory Comput 2012;8:618–28. [PubMed: 26596610]

135. Nguyen PT, DeMarco KR, Vorobyov I, Clancy CE and Yarov-Yarovoy V. Structural basis for antiarrhythmic drug interactions with the human cardiac sodium channel. Proceedings of the National Academy of Sciences of the United States of America. 2019;116:2945–2954. [PubMed: 30728299]

136. Yu Z, IJzerman AP and Heitman LH. K(v)11.1 (hERG)-induced cardiotoxicity: a molecular insight from a binding kinetics study of prototypical K(v)11.1 (hERG) inhibitors. Brit J Pharmacol. 2015;172:940–955. [PubMed: 25296617]

137. Davis AM, Webborn PJ and Salt DW. Robust assessment of statistical significance in the use of unbound/intrinsic pharmacokinetic parameters in quantitative structure-pharmacokinetic relationships with lipophilicity. Drug Metab Dispos. 2000;28:103–6. [PubMed: 10640503]

138. Neves P, Leite A, Rangel M, de Castro B and Gameiro P. Influence of structural factors on the enhanced activity of moxifloxacin: a fluorescence and EPR spectroscopic study. Anal Bioanal Chem. 2007;387:1543–52. [PubMed: 17200861]

139. Allen TW, Andersen OS and Roux B. Structure of gramicidin a in a lipid bilayer environment determined using molecular dynamics simulations and solid-state NMR data. J Am Chem Soc. 2003;125:9868–77. [PubMed: 12904055]

140. Crouzy S, Woolf TB and Roux B. A molecular dynamics study of gating in dioxolane-linked gramicidin A channels. Biophysical journal. 1994;67:1370–1386. [PubMed: 7529578]

141. Wang Y, Guo J, Perissinotti LL, Lees-Miller J, Teng G, Durdagi S, Duff HJ and Noskov SY. Role of the pH in state-dependent blockade of hERG currents. Sci Rep 2016;6:32536. [PubMed: 27731415]

142. Mitcheson JS, Chen J, Lin M, Culberson C and Sanguinetti MC. A structural basis for drug-induced long QT syndrome. Proceedings of the National Academy of Sciences of the United States of America. 2000;97:12329–33. [PubMed: 11005845]

NOVELTY AND SIGNIFICANCE

What Is Known?

- Cardiotoxicity in the form of deadly abnormal arrhythmia is one of the most common and dangerous drug risks.
- There is no current drug-screening tool that can distinguish therapies that may promote cardiac arrhythmias from chemically similar safer drugs.
- Current approaches rely on surrogate markers such as action potential duration or QT interval prolongation on the ECG.

What New Information Does This Article Contribute?

- We demonstrate a novel computational pipeline that connects the hugely disparate space and time scales of ion channel structure and function and predicst drug impact from the atom to the rhythm.
- Predictive models at the level of cell and tissue exposes fundamental arrhythmia vulnerability mechanisms and complex interactions underlying emergent behaviors.
- Human clinical data used for model validation showed excellent agreement, demonstrating the feasibility of the approach for cardiotoxicity prediction.

Drugs that share the common property of blocking the hERG potassium channel with consequent prolongation of the cellular action potential and QT interval on the ECG are deemed likely to be unsafe. However, hERG block and QT prolongation alone are not selective indicators for cardiac arrhythmia. In order to move beyond the current screening paradigm, we present a new approach that can predict the impact of a drug on the cardiac rhythm starting from the drug chemistry to distinguish between safe and unsafe hERG blockers. We utilized the cryo-EM structure of the hERG K^+ channel to develop and validate an atomistic structural model of the open conducting state. We then developed and validated structural atomistic models of dofetilide and moxifloxacin, hERG blockers differing pro-arrhythmia risk profiles. All-atom molecular dynamics simulations were used to probe dofetilide and moxifloxacin interactions with the open hERG channels. We connected atomistic scale information to protein, cell and tissue scales by using predicted drug binding affinities to model drug effects on hERG channel function. Model components were integrated into cell and tissue scale models to expose arrhythmia vulnerability mechanisms and emergent behaviors. Model outputs were validated with human clinical data and showed excellent agreement, demonstrating feasibility.

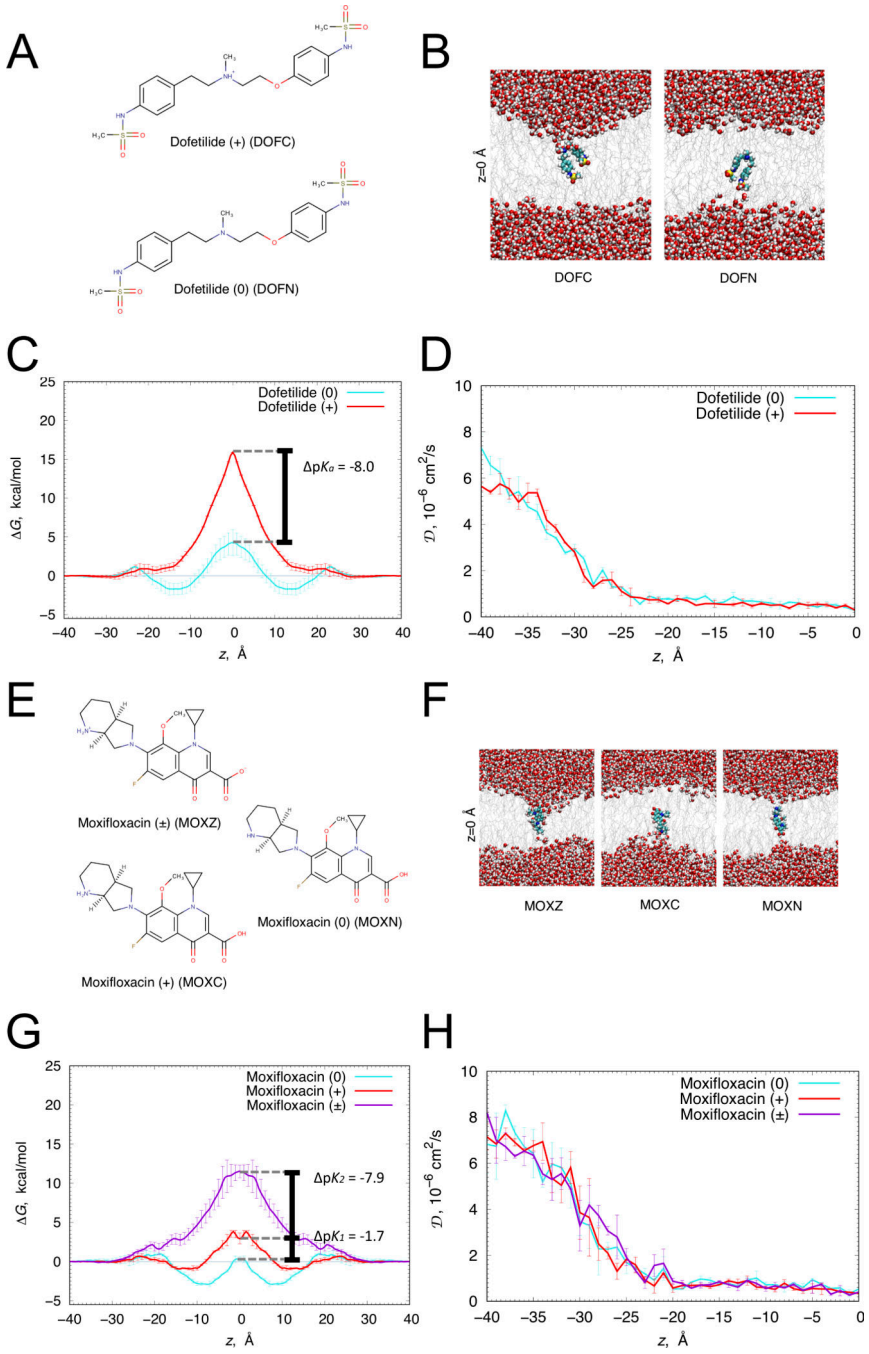

Figure 1. Translocation of dofetilide and moxifloxacin across a hydrated lipid membrane.

(A) Chemical structures of cationic (top) and neutral (bottom) dofetilide. **(B)** Representative snapshots of dofetilide at the center of POPC bilayer ($z = 0$) from umbrella sampling molecular dynamics simulations. Dofetilide and water molecule are in space-filling representation (C – cyan, O – red, N – blue, S – yellow, H – white), lipid tails are shown as gray sticks. **(C)** Free energy (ΔG) and **(D)** diffusion coefficient (D) profiles of neutral (cyan) and cationic (red) dofetilide crossing POPC membrane. **(E)** Zwitterionic (top), neutral (right) and cationic (bottom) moxifloxacin chemical structures. **(F)** Representative snapshots

of moxifloxacin at the center of DMPC bilayer ($z = 0$) from umbrella sampling molecular dynamics simulations. Moxifloxacin and water molecule are in space-filling representation (F – pink, C – cyan, O – red, N – blue, H – white), lipid tails are shown as gray sticks. **(G)** ΔG and **(H)** D profiles of zwitterionic (purple), neutral (cyan) and cationic (red) moxifloxacin crossing DMPC membrane. Error bars represent standard errors of mean computed based on profile asymmetries with respect to $z = 0$.

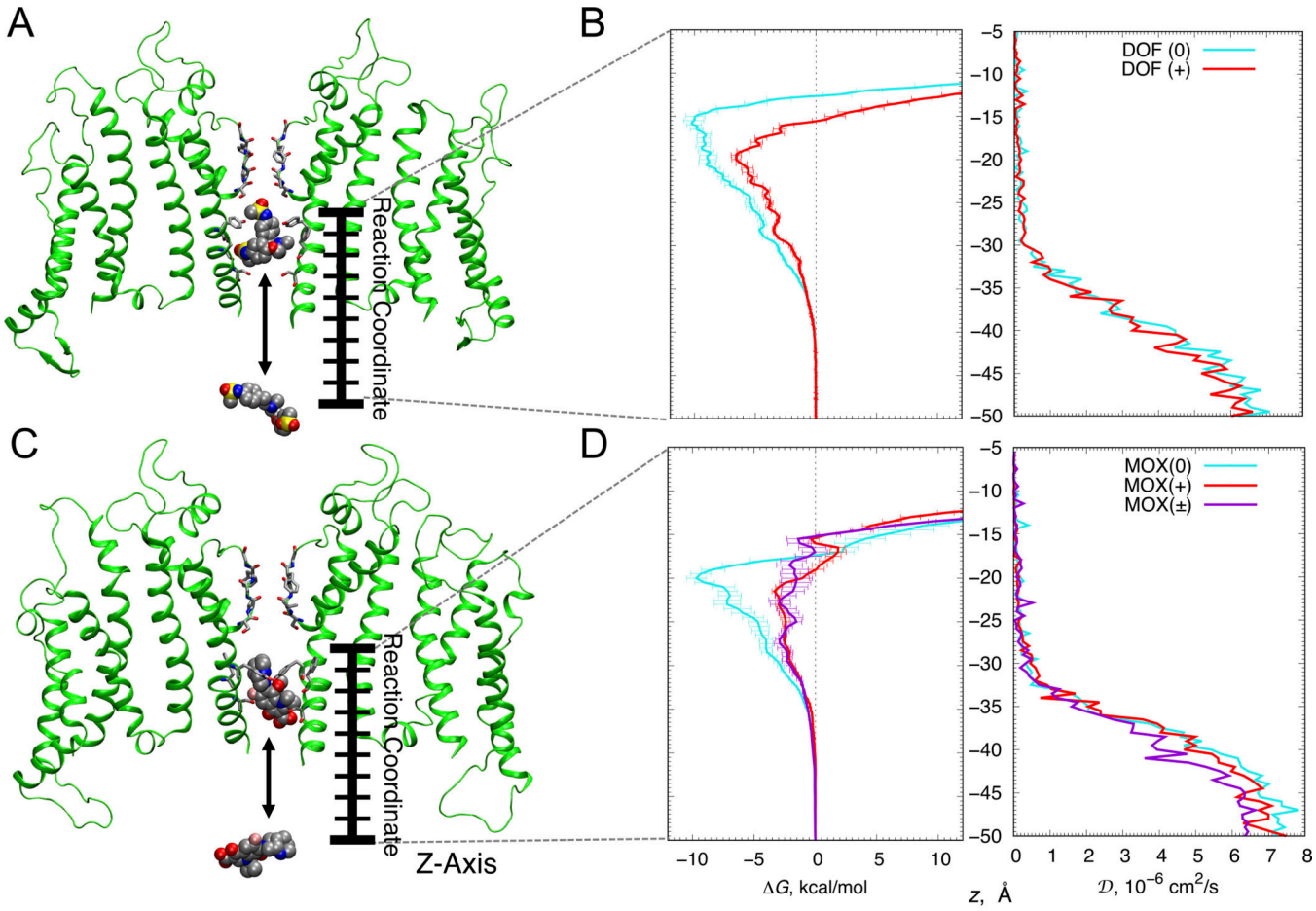

E

hERG Pore Binding Data					
	ΔG_{bind} (kcal mol^{-1})	K_D (μ M)	$\mathcal{D}_{pore}$ (10^{-6} cm^2 s^{-1})	k_{on} (μ M^{-1}s^{-1})	k_{off} (s^{-1})
Dofetilide (0)	-9.6	0.16	0.08	$6.7 \cdot 10^2$	$1.1 \cdot 10^2$
Dofetilide (+)	-5.9	65	0.15	$5.3 \cdot 10^2$	$3.5 \cdot 10^4$
Moxifloxacin (0)	-8.7	0.74	0.15	$6.6 \cdot 10^2$	$4.9 \cdot 10^2$
Moxifloxacin (+)	-3.1	6700	0.11	$4.2 \cdot 10^2$	$2.8 \cdot 10^6$
Moxifloxacin (±)	-2.9	8600	0.19	$3.4 \cdot 10^2$	$2.9 \cdot 10^6$

Figure 2. Open state hERG block by dofetilide and moxifloxacin.

(A, C) The representative open state hERG structures (two opposite chains shown as green ribbons) used to compute binding free energy (ΔG) and diffusion coefficient (D) profiles for dofetilide (panel A) and moxifloxacin (panel C). Drug molecules inside the hERG ßpore (top) and in bulk solvent (bottom) are in space-filling representation (C – gray, O – red, N – blue, S – yellow, F – pink, H – white), **(B, D)** ΔG (left) and D (right) profiles for dofetilide (panel B) and moxifloxacin (panel D) interactions, showing dominant binding wells of –10.1 kcal/mol and –6.6 kcal/mol at z = –15.5 Å and z = –20 Å for neutral (cyan) and cationic (red) dofetilide and –9.7 kcal/mol, –3.3 kcal/mol, and –2.9 kcal/mol at z = −20 Å, z = −21.5

Å and $z = -22.5$ Å, for neutral (cyan), cationic (red) and zwitterionic (purple) moxifloxacin. Error bars for ΔG profiles represent standard errors of mean computed from block averages. D values in the hERG pore (D_{pore}) of both dofetilide and moxifloxacin were comparable irrespective of drug ionization state as shown in panels B and D, right. **(E)** Drug binding affinities (ΔG_{bind} *and* K_D), diffusion coefficients (D_{pore}) and drug "on" (k_{on}) and "off" (k_{off}) rates computed from the umbrella sampling molecular dynamics simulations.

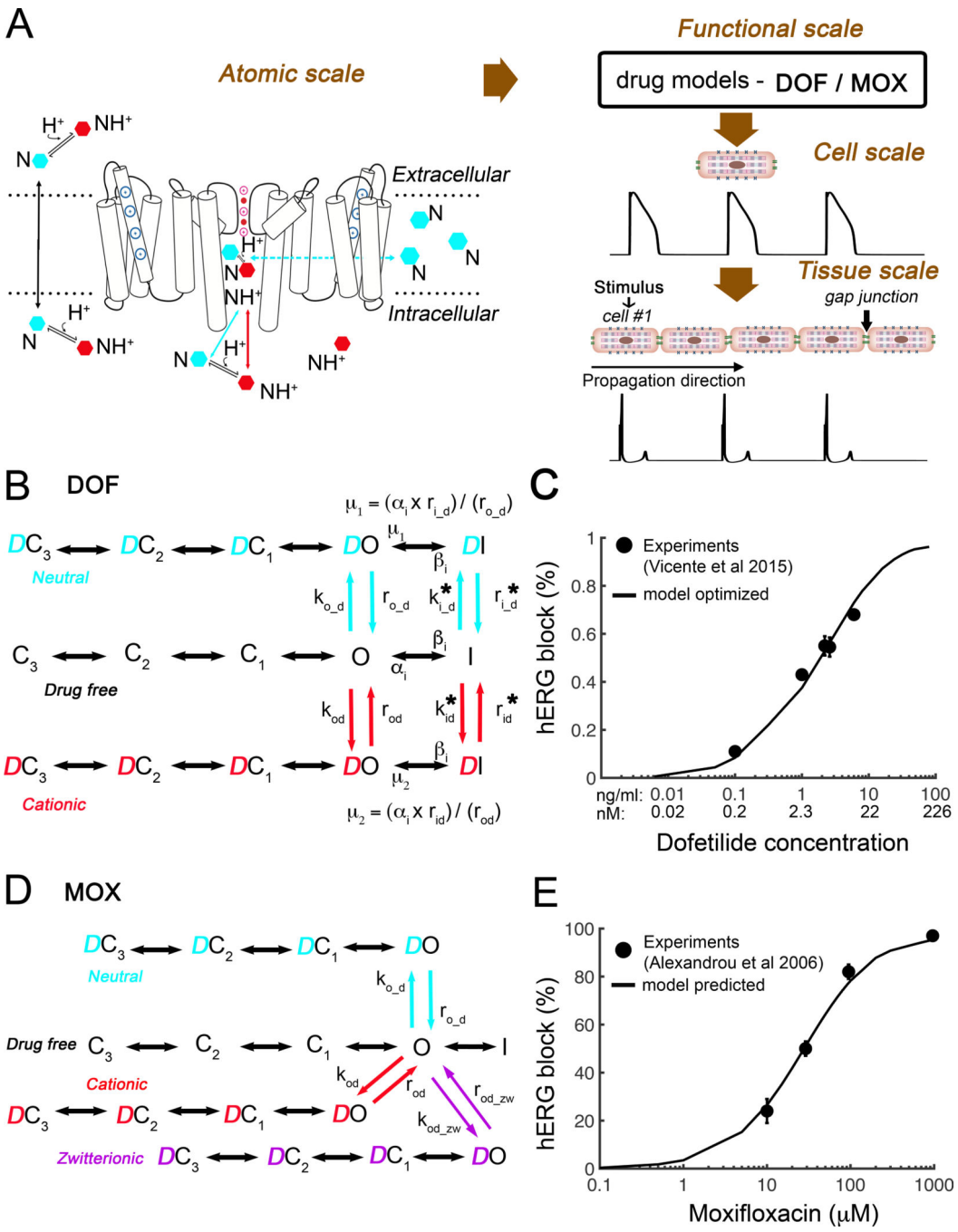

Figure 3. Concentration dependent block of hERG by dofetilide and moxifloxacin.

(A) Schematic diagram presents the connection of atomistic scale model of drugs interaction with the hERG channel (left) to the corresponding functional protein scale model (B and D) used in single-cell to tissue level simulations and computed pseudo ECG (bottom). **(B)** The Markov model represents a map of the hERG channel functional states. Drug free (black), cationic dofetilide bound (red) states, and neutral dofetilide bound (cyan) states are shown. **(C)** Experimentally measured dose dependent inhibition of hERG by dofetilide (black circles)[56] and optimized model-based results (black curve). **(D)** The Markov model of

hERG-moxifloxacin system: drug free (black), cationic drug bound (red) states, zwitterionic drug bound (purple), and neutral drug bound (cyan) states are shown. **(E)** Experimentally measured dose dependent inhibition of hERG by moxifloxacin (black circles)[20] and model predicted results (black curve).

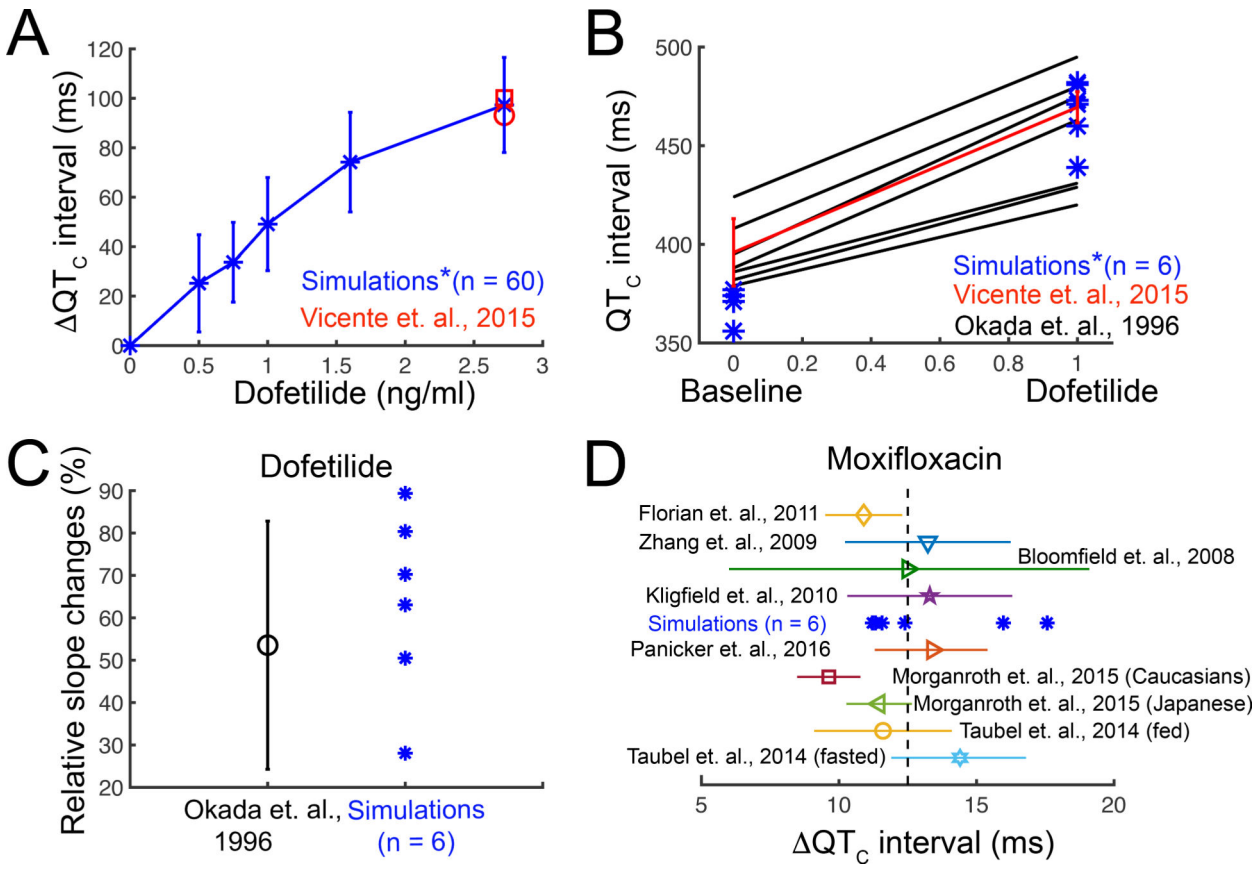

Figure 4. Validation of the drugs computational screening pipeline prototype with human clinical data

(A) Heart rate corrected pseudo ECG (ΔQT_C interval) was computed from a 1-dimensional strand of O'Hara-Rudy human cardiac ventricular myocytes for pacing frequencies between 43 – 75 bpm for a range of dofetilide concentrations (blue) compared to clinical data (red). **(B)** Comparison of human clinical data showing control and dofetilide affected rate corrected QT intervals[10, 56] (black and red lines) and simulated mean values under the same conditions (blue asterisks). Red line: two subjects received a single dose of 0.5 mg (population's mean maximum concentration C_{max} is 2.7±0.3 ng/mL). Blue asterisks (*): concentration 2.72 ng/mL (~6.16 nM) was used in the simulations. Black lines: subjects received 0.5 to 0.75 mg twice a day. **(C)** The clinically observed and *in silico* prediction of QT intervals over a wide range of preceding RR intervals after 2.72 ng/mL dofetilide application. Rate dependent changes in the QT interval were tracked as the slope of the linear regression line estimating the QT – $\sqrt{RR}$ relation. **(D)** Model predicted ΔQT_C intervals with 2.5 mg/L moxifloxacin application (blue asterisks). Color symbols with error bars: clinical data after 400 mg moxifloxacin oral dose (maximum concentration C_{max} is between 2.3 to 3.7 mg/L).[59–65]

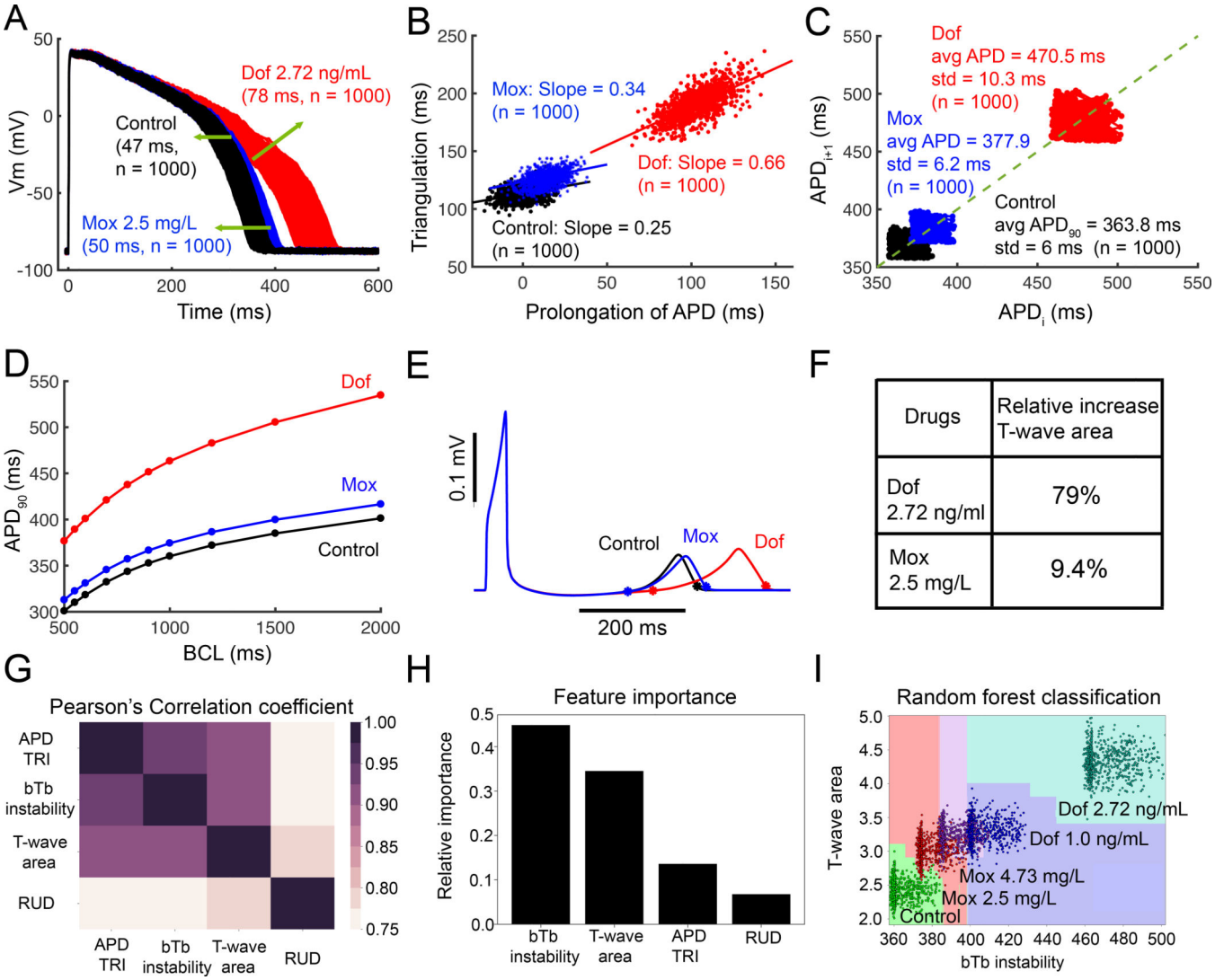

Figure 5. Computational screening for dofetilide and moxifloxacin induced arrhythmia vulnerability.

(A) Predicted *temporal APD dispersion* of 1000 simulated O'Hara-Rudy human ventricular action potentials generated after incorporating physiological noise to induce beat-to-beat (bTb) variability at 1 Hz in the drug-free control case and following simulated application of dofetilide (2.72 ng/mL), and moxifloxacin (2.5 mg/L). *Dispersion* of APD was quantified as the difference between the maximum and minimum of 1000 individual cells (Control = 47 ms; Moxifloxacin 2.5 mg/L = 50 ms; Dofetilide 2.72 ng/mL = 78 ms). **(B)** Action potential *triangulation* as a function of APD prolongation for individual cells for control (slope = 0.25), Moxifloxacin 2.5 mg/L (slope = 0.34), and Dofetilide 2.72 ng/mL (slope = 0.66) conditions **(C)** Simulated bTb *instability* of action potentials to small perturbations before and after application of drugs. Poincaré plots of sequential APD pairs indicating bTb instability are shown. **(D)** Action potential adaptation curves show APD_{90} at various pacing frequencies with or without dofetilide or moxifloxacin, demonstrating drug reverse use dependence. **(E)** Pseudo ECGs after a long pause (5000 ms) are shown for control,

moxifloxacin 2.5 mg/L, and dofetilide 2.72 ng/mL conditions. **(F)** Relative increased T-wave area by 79% with dofetilide 2.72 ng/mL, and 9.4% with moxifloxacin 2.5 mg/L. **(G)** The Pearson's correlation coefficients between paired TRIaD parameters. Pearson's coefficient value indicated by the color gradient, where 1 is highly correlated (black). **(H)** bTb *instability* emerged as the most important feature from the TRIaD parameters. **(I)** Classified regions for control (n = 1000), dofetilide 1 ng/mL (n = 1000), dofetilide 2.72 ng/mL (n = 1000), Moxifloxacin 2.5 mg/L (n = 1000), and Moxifloxacin 4.73 mg/L (n = 1000) using bTb *instability* and T-wave area.

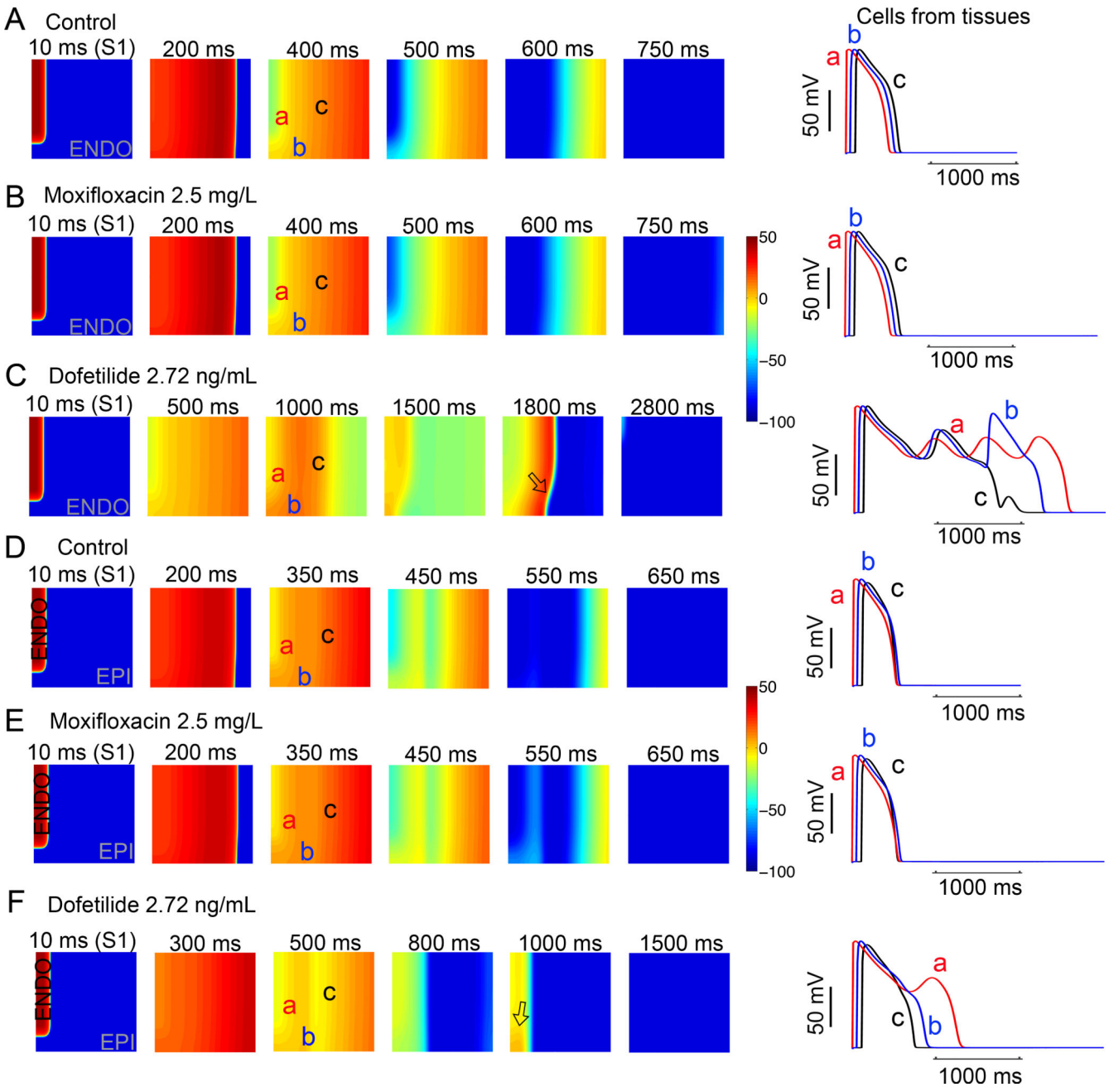

Figure 6. *In silico* diagnostic test in tissue reveals arrhythmia triggers with dofetilide and moxifloxacin.

Time snapshots (colored boxes) with voltage gradients are shown for two-dimensional simulated tissue (described in Supplemental Materials). Membrane voltages are indicated by the color gradient. Two-dimensional homogeneous (Panels A, B and C, endocardial cells) and heterogeneous (Panels D, E and F, endocardial region (cells 1 to 180) and epicardial region (cells 181 to 500)) anisotropic human ventricular *in silico* tissue (5 cm × 5 cm) composed of simulated myocytes. Single APs from sites ‘a’, ‘b’, and ‘c’ in the simulated tissues are shown in the right panels for each case.

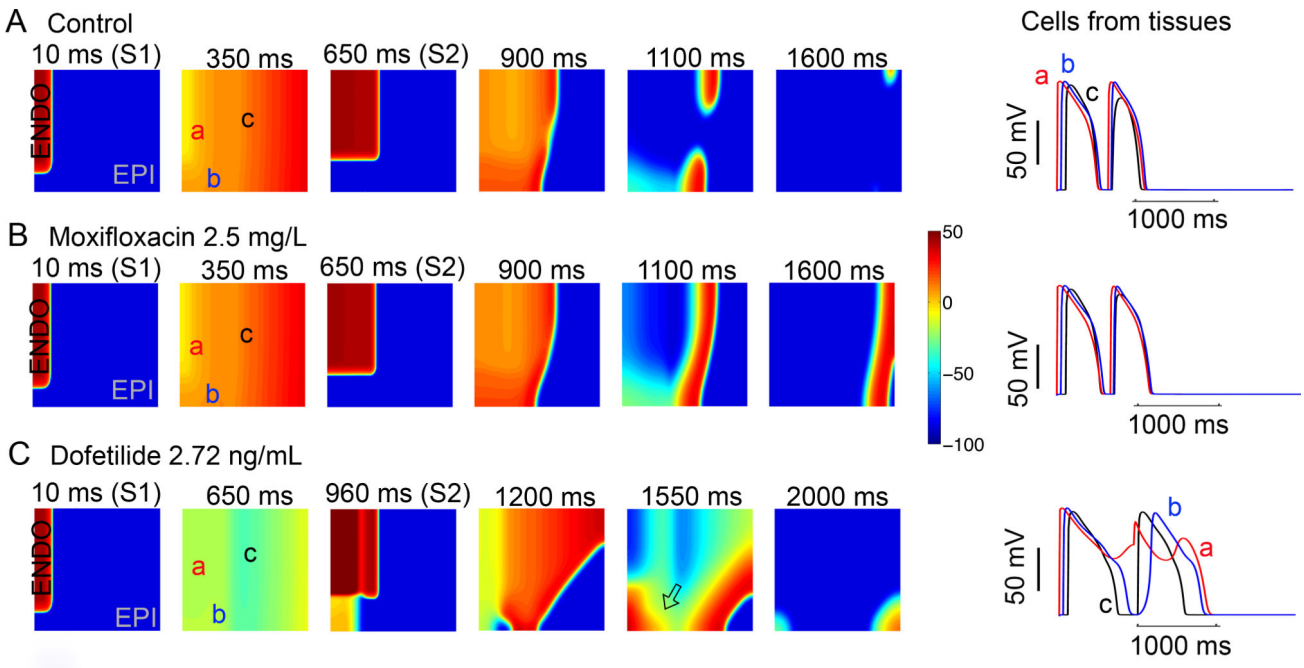

Figure 7. ***In silico*** **diagnostic test to reveal vulnerability to torsades de points arrhythmias by extrasystoles.**

Time snapshots (colored boxes) with voltage gradients are shown for two-dimensional simulated tissue as described below. Membrane voltages are indicated by the color gradient. The corresponding action potentials from three points in space (‘a’, ‘b’, and ‘c’) are shown in the right panels. **(A)** In the absence of drug (top row), arrhythmia triggers were not inducible. **(B)** Upon application of moxifloxacin (middle row), arrhythmia triggers were not inducible. **(C)** In the bottom row the effect of dofetilide is shown: numerous arrhythmia triggers were observed as afterdepolarizations and spatial repolarization gradients in underlying cellular action potentials (right). Single APs from site ‘a’, ‘b’, and ‘c’ in the simulated tissues are shown in the right panels for each case.

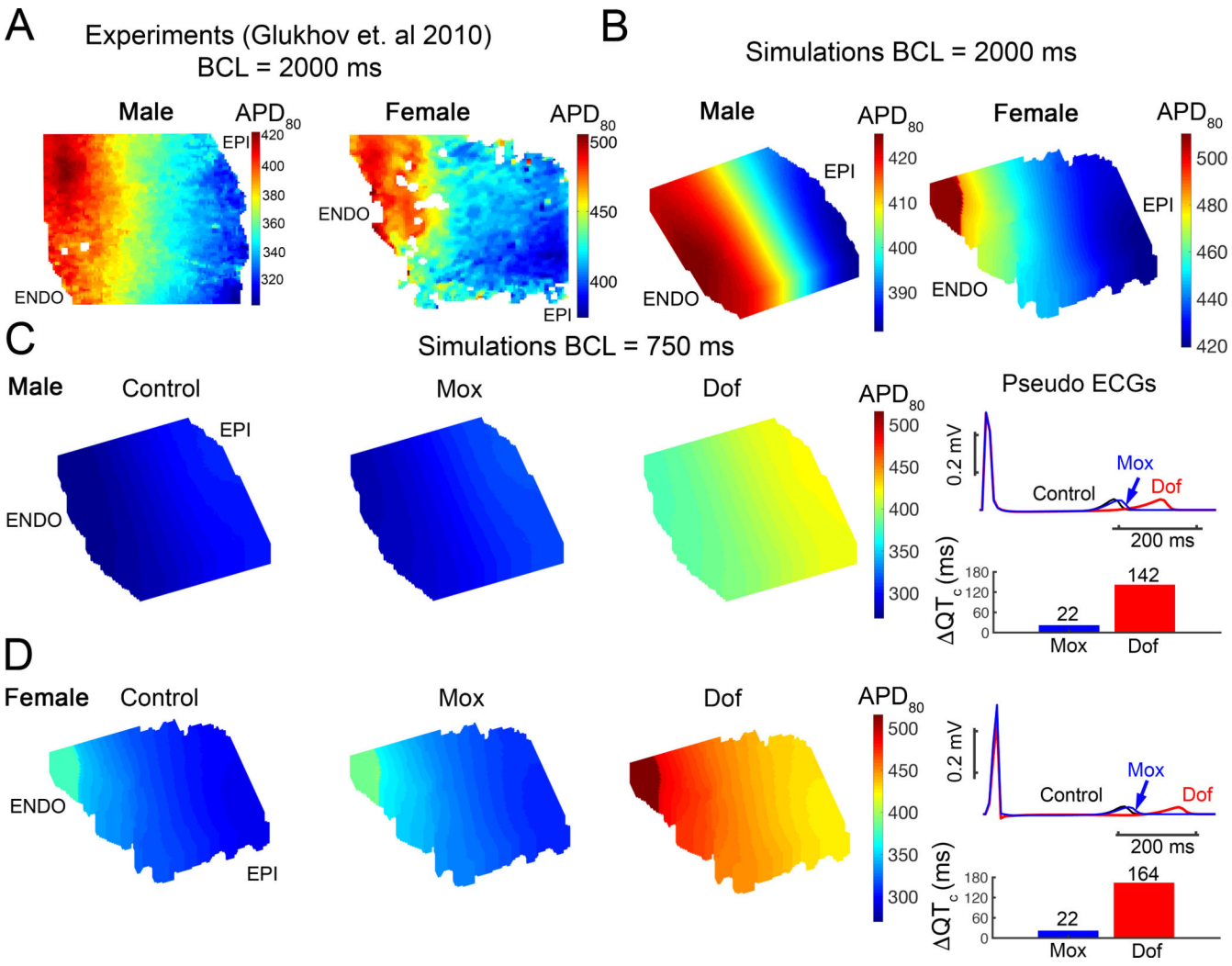

Figure 8. Predicted impact of sex as a biological variable with *in silico* 3D reconstructed left ventricular (LV) wedge based on Glukhov et al. [71] paced with before and after drug application.

(A) Experimental data from normal human female (right) and male (left) left ventricle [71]. **(B)** *In silico* reconstructed human tissues from these data from normal explanted heart at a pacing cycle length of 2000 ms (male – left and female – right). **(C)** The LV wedges were paced at basic cycle of 750 ms for 20 beats. The APD_{80} map was shown for male in the control condition (no drug) (left map in C) and following moxifloxacin (middle map) and dofetilide (right map) applications. Pseudo ECGs (the 20th beat) shows the effect of drug application on QT interval in the right panel. **(D)** Shown for female as in (C).